Journal of Extracellular Vesicles

RESEARCH ARTICLE OPEN ACCESS

Therapeutic Poxviruses Induce the Secretion of Immunostimulating and Anti-Tumoral Extracellular Vesicles

Lucas Walther[1,2,3,4,5,6] | Vincent Mittelheisser[1,2,3,4,5] | Marie-Christine Claudepierre[6] | Louis Bochler[1,2,3,4,5] | Magali Rompais[8] | Jules Deforges[6] | Nathalie Silvestre[6] | Annabel Larnicol[1,2,3,4,5] | Christine Carapito[8] | Eric Quémeneur[6,7] | Jacky G Goetz[1,2,3,4,5] | Karola Rittner[6] | Vincent Hyenne[1,2,3,4,5,9]

[1]Tumor Biomechanics, University of Strasbourg, Strasbourg, France | [2]INSERM UMR_S1109, University of Strasbourg, Strasbourg, France | [3]Université de Strasbourg, Strasbourg, France | [4]Fédération de Médecine Translationnelle de Strasbourg (FMTS), University of Strasbourg, Strasbourg, France | [5]Équipe Labellisée Ligue Contre le Cancer, Paris, France | [6]Transgene SA, Parc d'innovation, Illkirch-Graffenstaden, France | [7]Inserm, Agence de Programmes de Recherche en Santé, Paris, France | [8]Laboratoire de Spectrométrie de Masse Bio-Organique (LSMBO), Université de Strasbourg, Strasbourg, France | [9]CNRS, SNC5055, Strasbourg, France

Correspondence: Jacky G Goetz (jacky.goetz@inserm.fr) | Karola Rittner (rittner@transgene.fr) | Vincent Hyenne (hyenne@unistra.fr)

Received: 22 September 2025 | **Revised:** 13 April 2026 | **Accepted:** 7 May 2026

Keywords: antitumor vaccine | extracellular vesicles | poxvirus | secretome | therapeutic virus

ABSTRACT

Poxvirus-based vectors provide a versatile cancer immunotherapy platform, enabling the expression of immunostimulatory molecules and cancer-specific antigens. While infections with pathogenic viruses are well known to modulate extracellular vesicle (EV) biogenesis and function, the extent to which therapeutic poxviral vectors influence EV secretion by immune cells and thereby affect therapeutic efficacy remains underexplored. In this study, we showed that poxviruses, including the clinically relevant Modified Vaccinia Ankara (MVA), stimulate the secretion of small EVs (sEVs) containing viral proteins and immune-related signatures from peripheral blood mononuclear cells (PBMCs). Using an engineered MVA vector, we demonstrated the transfer of virus-encoded therapeutic payloads to sEVs, including the model ovalbumin (OVA)-derived peptide SIINFEKL presented by the class I major histocompatibility complex (MHC I) and the immune activators interleukin-12 (IL-12) and CD40 ligand (CD40L). Depending on the isolation method, these sEVs stimulated SIINFEKL-specific $CD8^+$ T cells with varying efficiencies in vitro. Remarkably, intravenous injection of these sEVs, but also of the soluble secretome from the same cells, into E.G7-OVA lymphoma–bearing mice reduced tumor growth to an extent comparable to the virus itself. Taken together, our findings indicate that EVs released from immune cells infected with engineered therapeutic poxviruses exert potent antitumor activity. These vesicles represent actionable mediators whose secretion and functionalization can be harnessed to improve viral vector–based immunotherapies, as well as being considered as therapeutic vectors in their own.

Jacky G Goetz, Karola Rittner and Vincent Hyenne contributed equally to this work

This is an open access article under the terms of the Creative Commons Attribution-NonCommercial-NoDerivs License, which permits use and distribution in any medium, provided the original work is properly cited, the use is non-commercial and no modifications or adaptations are made.
© 2026 The Author(s). *Journal of Extracellular Vesicles* published by Wiley Periodicals, LLC on behalf of the International Society for Extracellular Vesicles.

1 | Introduction

Virus-based vectors, including lentiviruses, adenoviruses and poxviruses (Bezeljak 2022; Bendjama and Quemeneur 2017), have emerged as a versatile and clinically validated platform for gene delivery, oncolytic virotherapy, and therapeutic vaccination in oncology. For instance, engineered poxviral vectors eradicate tumors by (i) enhancing tumor tropism; (ii) conferring tumor-selective replication (Foloppe et al. 2019); (iii) expressing tumor-associated antigens (TAAs) or (iv) delivering immunostimulatory molecules (Travieso et al. 2022). They also support therapeutic cancer vaccination, including personalized neoantigen constructs that elicit robust, patient-tailored immune responses (Seclì et al. 2023). Among them, the Modified Vaccinia Ankara (MVA) is an attenuated poxvirus strain that has been extensively investigated and demonstrated to be a safe, flexible, and immunogenic vector (Cottingham et Carroll 2013). In preclinical studies, MVA vaccination was shown to induce the generation of tumor antigen-specific $CD8^+$ T cells able to trigger a complete regression of tumors (Ramos et al. 2022). The MVA-based personalized vaccine TG4050 targeting neoantigens in head and neck cancer is currently under clinical evaluation (ClinicalTrials.gov identifier NCT04183166). Yet the full consequences of therapeutic virus infection, both on the infected immune cells and the subsequent events leading to adaptive immunity activation, are incompletely understood. A deeper understanding of how therapeutic viral infection remodels host cells and shapes systemic immunity will not only enable the development of safer and more effective treatments but also broaden our understanding of the mechanisms by which viruses modulate infection efficacy, together with the magnitude and quality of the elicited immune response. Notably, one broadly overlooked consequence of viral infection is the remodelling of extracellular vesicles (EVs) secretion and content, reflecting the complex, intertwined links between viruses and EV biogenesis pathways (Martin et al. 2024). EVs are heterogeneous particles delimited by a lipid bilayer (ranging from ≈30 nm to a few μm) and secreted by most cells via different pathways, from endosomes or from the plasma membrane (Van Niel et al. 2018). As mediators of intercellular communication in physiology and disease (e.g., inflammation, cancer, cardiovascular disorders), EVs transport lipids, proteins and nucleic acids (RNA, DNA), with cargo composition reflecting the state and identity of the donor cell (Kalluri et LeBleu 2020). On a translational level, EVs are being used both as circulating disease biomarkers and developed as versatile delivery vehicles for bioactive therapeutics (Kumar et al. 2024), notably in cancer, with growing emphasis on engineering for improved drug delivery and immunomodulation (Yang et al. 2024; Mohamed et al. 2025). Since EVs play a major role in modulating immune responses (Buzas 2023), notably by presenting antigens at their surface to activate T cells (Greening et al. 2023), they emerged as vaccination vectors. Viruses are ontogenetically, structurally and functionally closely related to EVs (Cortes-Galvez et al. 2023; Moulin et al. 2023) and exploit their secretion mechanisms to their advantage (Hassan et al. 2021; Chatterjee et al. 2024). For instance, the vaccinia virus (strain WR) hijacks the endosomal sorting complex required for transport (ESCRT)-mediated multivesicular body (MVB) pathway, known to be involved in cargo sorting and exosome secretion (Xu et al. 2023), for its egress from the cell (Huttunen et al. 2021). As a consequence, infected cells secrete a variety of particles forming a continuum, ranging from unaltered host-derived EVs to fully infectious viral particles, with intermediates such as virus-induced EVs and virus-like particles (Nolte-'t Hoen et al. 2016). For instance, cells infected with an MVA encoding the immunostimulatory molecule CD40L release EVs displaying both the viral envelope protein B5 and CD40L on their surface (Spehner and Drillien, 2008).

Based on these observations, we wondered whether (i) immunomodulatory therapeutic poxviruses could influence both the secretion and content of EVs secreted by infected immune cells and (ii) such EVs may contribute functionally to the efficacy of anti-tumoral therapeutic vaccines. To test these hypotheses, we used three members of the *Poxviridae* family exploited for therapeutic purposes: the *Vaccinia Virus* (strain Copenhagen, VV_{COP}) which is replication-competent; the MVA, an attenuated strain replication-deficient in most mammalian cells, and the Pseudocowpox virus (PCPV) that replicates efficiently in bovine cells. We first established a method to successfully separate EVs secreted by PBMCs, either infected with VV_{COP} or MVA, from closely related viral particles, based on size filtration and ultracentrifugation (UC). Then, using this protocol, we characterized *in vitro* and *in vivo* the content and function of virus-free small EVs (sEVs) secreted by PBMCs or murine dendritic cells (DC) DC2.4 infected with surrogates MVA vectors used for preclinical studies, either encoding reporter gene eGFP (MVA-eGFP) or therapeutic payloads (^{armed}MVA). We demonstrated that infection with the ^{armed}MVA stimulates the release of sEVs loaded with MVA-encoded immunomodulatory payloads which prevent tumor progression *in vivo*. Our results suggest that EVs partially mediate the therapeutic effect of immunostimulatory poxviruses, paving the way for improved virus-based therapies by tuning EV-mediated functions or directly using EVs as therapeutic vehicles.

2 | Methods

2.1 | Cell Culture

2.1.1 | Human Primary Cells

Leucocyte concentrates (buffy coats) from healthy donors were provided by the Etablissement Français du Sang (EFS), Strasbourg, France. Human PBMCs were isolated by standard density gradient centrifugation using Ficoll–Paque PLUS (GE Healthcare, Sweden) in 50 mL Blood Separation Tubes (Dacos, Denmark). PBMCs were cultured in RPMI-1640 medium (Sigma) supplemented with 10% heat-inactivated fetal bovine serum (FBS) (#35–070-CV, Corning), 2 mM L-glutamine (Sigma) and 40 μg/mL gentamycin (Sigma) at 37°C and 5% CO_2. Heat-inactivated FBS was heated for 30 min in a 56°C water bath to inactivate complement.

2.1.2 | Cell Lines

DC2.4 (#SCC142, Merck) are immortalized murine DC, originally created by transducing bone marrow isolates of C57BL/6

20013078, 2026, 6, Downloaded from https://isevjournals.onlinelibrary.wiley.com/doi/10.1002/jev2.70307 by Cochrane France, Wiley Online Library on [19/06/2026]. See the Terms and Conditions (https://onlinelibrary.wiley.com/terms-and-conditions) on Wiley Online Library for rules of use; OA articles are governed by the applicable Creative Commons License

mice with retrovirus vectors expressing murine granulocyte-macrophage CSF (GMCSF) and the myc and raf oncogenes. DC2.4 exhibits characteristic features of DC, including cell morphology and the expression of dendritic cell-specific markers and the ability to phagocytose and present exogenous antigens on both MHC class I and class II molecules (Shen et al., 1997). DC2.4 cells were cultured in RPMI-1640 (Sigma) supplemented with 10% heat-inactivated FCS (#35–070-CV, Corning), 2 mM L-glutamine, 40 µg/mL gentamycin, 1x MEM non-essential amino acids (Gibco), and 1x HEPES Buffer (Gibco) at 37°C and 5% CO_2.

E.G7-OVA cells (ATCC, CRL-2113) are murine T lymphoblast cell line derived from the C57BL/6 (H-2 b) mouse lymphoma cell line EL4. E.G7-OVA cells were cultured in RPMI-1640 medium (Sigma), supplemented with 10% heat-inactivated FCS (#35–070-CV, Corning), with 2 mM L-glutamine adjusted to contain 1.5 g/L sodium bicarbonate, 4.5 g/L glucose, 10 mM HEPES and 1.0 mM sodium pyruvate and supplemented with 0.4 mg/mL G418, (all provided by Sigma) at 37°C and 5% CO_2.

U-2OS cells (ATCC, HTB-96) are derived in 1964 from a moderately differentiated osteosarcoma of the tibia of a 15-year-old, White, female patient, they were cultured in DMEM (Gibco), supplemented with 10% FCS (#35–070-CV, Corning), 2 mM L-glutamine (Sigma) and 40 µg/mL gentamycin (Sigma) at 37°C and 5% CO_2.

BHK-21 cells (ATCC, CCL-10) are fibroblasts isolated from the kidney of an uninfected golden hamster, they were cultured in DMEM High Glucose (Gibco), supplemented with 10% FCS (#35–070-CV, Corning) at 37°C and 5% CO_2.

BT cells (CRL-1390) are bovine *Bos Taurus* turbinate cells, they were cultivated in DMEM supplemented with 10% fetal horse serum (Hyclone, Logan, USA), 2 mM L-glutamine (Sigma) and 40 mg L^{-1} gentamicin (Sigma).

Regular mycoplasma testing was carried out for all cell lines (Clean Cells, Vendée, France or Taconic Biosciences).

2.2 | Viral Vectors

All viruses were generated by homologous recombination and amplified in chicken embryo fibroblast (CEF) for VV_{COP} and MVA or in BT cells for PCPV. Cells were transfected with the shuttle plasmids encoding the expression cassettes (described below) and previously infected with parental virus. Recombinant viruses were isolated by picking non-fluorescent viral plaques. The identity and integrity of expression cassettes were checked by PCR analysis and DNA sequencing of each locus. All viruses were purified by tangential flow filtration and titrated by plaque assay.

The following vectors were previously described: VV_{COP}-eGFP (Foloppe et al. 2019). MVA-eGFP and ^{empty}MVA (Fournillier et al. 2007; Erbs et al. 2008), PCPV-eGFP (Ramos et al. 2022). OVA MVA, OVA-IL12 MVA, OVA-CD40L MVA and OVA-CD40L-IL12 (corresponding to the ^{armed}MVA), shown in Figure S4, encode their respective payloads: a polyepitope cassette comprising two MHC I–restricted epitopes (SIINFEKL, $OVA_{257–264}$/H-2K^b; WMHHNMDLI/H-2D^b) and two MHC II–restricted epitopes (ISQAVHAAHAEINEAGR, $OVA_{323–339}$/I-A^b; NAGFNSNRANSSRSS/I-A^b) fused to eGFP under the pH5R promoter in deletion III, murine CD40L under the pH5R promoter in deletion II and murine IL-12 under the early/late 11K7,5 promoter in deletion II.

2.3 | Cell Culture Conditions for EVs Production

PBMCs were cultured in complete medium for testing the various isolation methods described with VV_{COP}-eGFP. When using MVA-eGFP with PBMCs for mass spectrometry analysis of EVs content and all experiments involving DC2.4, cells were cultured in EV-depleted medium that was prepared using proper 2x complete medium, ultracentrifuged at 100,000 g for 18 h (Beckman Coulter Optima XL-80K Ultracentrifuge with a SW28 rotor) to remove EVs from FBS. The resulting supernatant was adjusted to 1× with the appropriate serum-free medium for each cell type.

2.4 | Cell Infection

PBMCs were infected with virus of interest at MOI = 1 and incubated for 18 h, and DC2.4 were infected with virus of interest at MOI = 1 and incubated for 18 h, before harvesting the supernatant containing EVs.

2.5 | EVs Isolation and Quantification

After infection and incubation, supernatant was pre-cleared by centrifugation at 300 g for 10 min and 2,000 g for 30 min, at room temperature.

3 | UC

Pre-cleared supernatant was centrifuged at 10,000 g for 45 min at room temperature before a final UC (Beckman Coulter Optima XL-80K Ultracentrifuge in 38.5 mL Open-Top Thinwall Polypropylene tubes with a SW28 rotor, Beckman Coulter) at 100,000 g for 2 h, at 4°C. The supernatant was discarded and resulting EVs pellet was resuspended in PBS and stored at 4°C.

4 | Immunocapture

Pre-cleared supernatant was centrifuged at 10,000 g for 45 min at room temperature and EVs were isolated using the EV Isolation Kit Pan (#130-110-912, Miltenyi Biotec), according to the manufacturer's instructions. Two fractions were obtained: the FT, corresponding to the flowthrough fraction containing non-bound components to MicroBeads, and the CAPT. fraction, corresponding to eluted EVs (and other co-purified particles) bound to MicroBeads and retained prior elution.

20013078, 2026, 6, Downloaded from https://isevjournals.onlinelibrary.wiley.com/doi/10.1002/jev2.70307 by Cochrane France, Wiley Online Library on [19/06/2026]. See the Terms and Conditions (https://onlinelibrary.wiley.com/terms-and-conditions) on Wiley Online Library for rules of use; OA articles are governed by the applicable Creative Commons License

5 | Iodixanol Density Gradient

Pre-cleared supernatant was concentrated using a Centricon Plus-70 10 kDa (#UFC701008, Merck Millipore) according to the manufacturer's instructions. An iodixanol gradient (Optiprep™ 60% iodixanol (w/v), Serumwerk Bernburg, Germany) was used as described by Van Deun et al. 2014. Briefly, the gradient was formed by gently layering 4 mL of 40%, 4 mL of 20%, 4 mL of 10% and 3.5 mL of 5% iodixanol solutions on top of each other in a 17 mL polypropylene tube (Beckman Coulter). 1 mL of concentrated sample was overlaid on the top of the gradient which was then centrifuged for 18 h at 100,000 g and 4°C (Beckman Coulter XL-70 centrifuge with a SW 32.1 Ti rotor). To prevent disturbance of gradient, deceleration was performed without applying brakes. 16 fractions of 1 mL and 1 fraction of 0.5 mL were collected from the top to the bottom of the gradient, diluted in PBS and centrifuged for 3 h at 100,000 g and 4°C. After discarding the supernatant, the resulting pellets were resuspended in 100 µL PBS and stored overnight at 4°C before being analysed by NTA and titration assays.

6 | Iodixanol Velocity Gradient

Pre-cleared supernatant was concentrated using a Centricon Plus-70 10 kDa (#UFC701008, Merck Millipore) according to the manufacturer's instructions. An iodixanol gradient (Optiprep™ 60% iodixanol (w/v), Serumwerk Bernburg, Germany) was used as described by Martin-Jaular et al., 2021. Briefly, each solution was prepared by diluting Optiprep™ in PBS to the indicated iodixanol concentration, and the gradient was formed by gently layering 3 mL of 18%, 3 mL of 14%, 3 mL of 10% and 2.5 mL of 6% iodixanol solutions on top of each other in a 13 mL polyallomer tube (Beckman Coulter). 1 mL of concentrated sample was overlaid on the top of the gradient which was then centrifuged for 1 h at 200,000 g and 4°C (using a Beckman Coulter XL-70 centrifuge with a SW 32.1 Ti rotor). To prevent disturbance of gradient, deceleration was performed without applying brakes. 12 fractions of 1 mL and 1 fraction of 0.5 mL were collected from the top to the bottom of the gradient, diluted in PBS and centrifuged for 45 min at 100,000 g and 4°C. After discarding the supernatant, the resulting pellets were resuspended in 100 µL PBS and stored overnight at 4°C before being analysed by NTA and titration assays.

7 | Filtration

Pre-cleared supernatant was concentrated using a Centricon Plus-70 10 kDa (#UFC701008, Merck Millipore) at room temperature, according to the manufacturer's instructions. Concentrated samples remained unfiltered or were passed through filters with 200 nm (0,2 µm, SFCA, 25 mm, #723–2520, Nalgene) or 100 nm (Millex 0,1 µm, PVDF, 33 mm, #SLVV033RS, Merck Millipore) pores and EVs were either recovered by UC or SEC afterward.

8 | SEC

When tested as a standalone isolation method, the first generation of qEV2 70 nm Legacy columns (Izon Science Ltd, New Zealand) were used according to the manufacturer's instructions. In brief, pre-cleared supernatant was concentrated using a Centricon Plus-70 10 kDa (#UFC701008, Merck Millipore). After rinsing the column with PBS, 2 mL of concentrated sample were loaded before adding 12 mL of PBS; this void volume was discarded. Then, 2 mL of PBS were successively added to harvest ten fractions of 2 mL. Each fraction was stored overnight at 4°C before being analysed by NTA and titration assays.

When used to recover EVs after 100 nm filtration and enhance their separation from soluble proteins, the qEV2 35 nm Gen 2 columns (Izon Science Ltd, New Zealand) were used according to the manufacturer's instructions. After rinsing the column with PBS, 2 mL of concentrated sample were loaded before adding 13.9 mL of PBS; this void volume was discarded. Then, 2 mL of PBS were successively added to harvest ten fractions of 2 mL. Fractions 1 to 4 were pooled to form the EVs fraction and fractions 5 to 10 were pooled to form the proteins-enriched fraction, before being concentrated using Amicon Ultra-15 Centrifugal Filter Unit 10 kDa (#UFC901024, Merck Millipore). The volume of both samples was equalized with PBS, analysed by NTA and stored at 4°C.

Unless otherwise stated, EVs for functional assays and in vivo experiments were quantified by NTA and either used immediately after isolation or stored overnight at 4°C; stored samples were analysed or injected the following day. For proteomic analyses by mass spectrometry EVs were quantified by NTA, aliquoted, and stored at −80°C until analysis.

9 | Nanoparticles Tracking Analysis (NTA)

According to the manufacturer's procedure, EVs (or particles) were diluted in PBS and the number of EVs (or particles) was determined using the ZetaView analyser (PMX-120) from Particle Metrix GmbH (Meerbuch, Germany). The sensitivity of the camera was set to 80 for all measurements. The data were analysed using the ZetaView analysis software version 8.05.16 SP7. The quantities of EVs (or particles) are expressed as the number of EVs (or particles)/secretory cells, counted when seeding the culture flasks just before infection.

9.1 | Infectivity Titration

Samples were titrated by plaque assays, performed on virus-specific indicator cells: U-2 OS (samples from VV_{COP}–infected PBMCs), BHK-21 (samples from MVA-infected PBMCs or DC2.4), and BT cells (samples from PCPV-infected PBMCs). Confluent monolayers in 6-well plates were inoculated with 10-fold serial dilutions of samples (duplicate wells), adsorbed for 30 min to 2 h at RT or 37°C (depending on the cell type) prior addition of medium containing agarose or carboxymethyl cellulose. Plates were incubated until plaques were countable (72 h for VV_{COP}; 30 h for MVA; 48 h for PCPV). Plaques were visualized by neutral red (PCPV) or crystal violet staining (VV_{COP}); or were revealed by immunostaining with an anti-vaccinia virus antibody (#B65101R, Meridian Bioscience) followed by an HRP-conjugated secondary (#P0448, Dako) and development with a chromogenic peroxidase substrate (MVA). PFU/mL were calculated from dilutions yielding 20–100 plaques.

20013078, 2026, 6, Downloaded from https://isevjournals.onlinelibrary.wiley.com/doi/10.1002/jev2.70307 by Cochrane France, Wiley Online Library on [19/06/2026]. See the Terms and Conditions (https://onlinelibrary.wiley.com/terms-and-conditions) on Wiley Online Library for rules of use; OA articles are governed by the applicable Creative Commons License

9.2 | Mass Spectrometry

EVs samples preparation: As described above, EVs were isolated by UC from PBMCs (cultured in EVs-free medium) that were either uninfected (mock) or infected with MVA encoding eGFP at MOI = 1. Four independent replicates were performed per condition (6 conditions; $n = 24$ total samples). For proteomics, 1×10^9 particles per sample were collected and stored at −80°C until mass-spectrometry analysis.

Electrophoresis and in gel trypsin digestion: Samples were lysed using 135 µL of Laemmli buffer. The whole material was loaded on an in-house poured 4% acrylamide stacking gel. Gel was stained with Coomassie Blue and the stacking bands were manually excised. Proteins were then reduced using 10 mM dithiothreitol and alkylated using 55 mM iodoacetamide before in-gel digestion overnight at 37°C with 0.2 µg of trypsin/LysC (Promega, Madison, USA). Peptides were extracted for 1 h with 90 µL of 80% acetonitrile, 0.1% formic acid. Peptide mixtures were then dried and resuspended in 50 µL water acidified with 0.1% formic acid.

Liquid Chromatography-Tandem Mass Spectrometry (LC-MS/MS) Analyses: LC-MS/MS analyses of peptide extracts were performed on a NanoElute LC-system coupled to a TimsTOF Pro mass spectrometer equipped with a CaptiveSpray ion source (Bruker Daltonics, Billerica, MA, USA). Mobile phase A was constituted of 97.9% water, 2 % acetonitrile and 0.1% formic acid and mobile phase B was constituted of 99.9% acetonitrile and 0.1% formic acid. A sample volume of 1 µL was loaded into an AcclaimPepMap C18 precolumn (0.1×20 mm, 5 µm particle size, ThermoFisher Scientific) at 120 bars and 2% B. This step was followed by reverse-phase separation at a flow rate of 300 nL/min using an Aurora 2 C18 separation column (250 mm x 75 µm id, 1.6 µm particle size, IonOpticks) and a gradient from 2% to 25% B in 90 min, from 25% to 35 % B in 10 min, from 35% B to 85% B in 13 min, and maintained at 85% B for 17 min. Precolumn and column were further reconditioned using 10 or 5 volumes of 2% B respectively.

The TimsTOF Pro instrument was operated in Data Dependent Acquisition-Parallel Accumulation Serial Fragmentation (DDA-PASEF) mode with 10 PASEF scans in a mass range from 100 m/z to 1700 m/z leading to 1.17 s cycle time. The ion mobility range scanned from 0.7 to 1.25 V.s/cm^2 with accumulation and ramp times of 100 ms. Peptides with a minimum intensity of 2500 were selected for fragmentation and were automatically added on a dynamic exclusion list for 0.4 min. Collisional induced dissociation (CID) voltage was tuned according to the mobility of the selected ion using a ramp from 20 eV for 0.6 V.s/cm^2 to 59 eV for 1.6 V.s/cm^2.

LC-MS/MS data interpretation and validation: Raw files were converted to .mgf peaklists using Data Analysis (version 5.3, Bruker Daltonics) and were submitted to Mascot database searches (version 2.6.2, MatrixScience, London, UK) against a multispecies protein database (total of 108,981 entries) including *Homo sapiens* and MVA virus sequences as target sequences, plus *Bos Taurus* and *Gallus gallus* as contaminant sequences, all extracted from UniProtKB-SwissProt and UniProtKB-TrEmbl. Benjamini Hochberg strategy was used to validate true identifications (Couté et al. 2020). Spectra were searched with a mass tolerance of 10 ppm in MS mode and 0.05 Da in MS/MS mode. One trypsin missed cleavage was allowed. Carbamidomethylation of cysteine residues was set as a fixed modification. Oxidation of methionine residues and acetylation of protein n-termini were set as variable modifications. Identification results were imported into Proline software (http://proline.profiproteomics.fr/; Bouyssié et al. 2020) for validation. Peptide Spectrum Matches (PSM) with pretty rank equal to one and a minimum length of 7 amino acids were retained. False Discovery Rate was then optimized to be below 1% at PSM level using Mascot score and below 1% at Protein Level using Fisher score.

Label Free Quantification: Peptide abundances were extracted thanks to Proline software version 1.0 (http://proline.profiproteomics.fr/; Bouyssié et al. 2020) using a m/z tolerance of 10 ppm. Alignment of the LC-MS runs was performed using Loess smoothing. No Cross assignment was allowed. The best 2+/3+/4+ peptide ion was used to assign an abundance to a peptide. Protein abundance was then computed by summing the abundance of all specific peptides.

Statistical Analysis: Protein abundances of human and viral proteins (2050 proteins) were loaded into Prostar software version 1.26.4 (http://www.prostar-proteomics.org/; Wieczorek et al. 2017) and associated to the 6 conditions (mock no filtration, mock filtered 200 nm, mock filtered 100 nm, MVA no filtration, MVA filtered 200 nm, MVA filtered 100 nm). Proteins with at least 3 values in at least one condition (3/4 replicates) were kept for further statistical analysis. Protein abundances were normalized using 15% quantile centering. Residual missing values were imputed in a conservative way (quantile 2.5%). Pairwised Student *t*-tests were performed to compare mock vs MVA infected cells according to the three filtration statuses.

P-values calibration was corrected using Benjamini-Hochberg method, and FDR was set to ∼1%–4%. More precisely, the comparison mock vs MVA without filtration leads to 0.95% FDR using *p*-values below 0.00209, the comparison mock vs MVA with 0.2 µm filter leads to 3.93% FDR using *p*-values below 0.00229, the comparison mock vs MVA with 0.1 µm filter leads to 2.63% FDR using *p*-values below 0.00182.

The mass spectrometry proteomics data have been deposited to the ProteomeXchange Consortium via the PRIDE partner repository (Perez-Riverol et al. 2022).

Proteins with $p < 0.01$ and log2FC ≥ 0.5 were retained for heat maps and volcano plots, generated with custom R functions and the R package Pheatmap. GO term analysis was performed using https://string-db.org/ and all proteins with -log(pValue) >1,3 were considered.

9.3 | EV Characterisation

9.3.1 | EV Surface Marker Profiling by Electrochemiluminescence (ECL) Immunoassay

Assays were performed on MSD 1-Spot High Binding SECTOR Plate (L15XB, Meso Scale Discovery) following the manufacturer's instructions. Wells were coated with 25 µL/well of samples

20013078, 2026, 6, Downloaded from https://isevjournals.onlinelibrary.wiley.com/doi/10.1002/jev2.70307 by Cochrane France, Wiley Online Library on [19/06/2026]. See the Terms and Conditions (https://onlinelibrary.wiley.com/terms-and-conditions) on Wiley Online Library for rules of use; OA articles are governed by the applicable Creative Commons License

solution, containing 2,5.10^8 EVs. Plates were sealed and incubated 2 h at room temperature (RT) without shaking. Plates were gently washed with 150 µL PBS/well, then blocked with 150 µL/well of PBS 5% Blocker A (R93BA, Meso Scale Discovery) for 1 h at RT with gentle orbital shaking. After a washing with 150 µL PBS/well, 25 µL/well of detection antibody solution (diluted at 1 µg/mL in PBS 5% Blocker A) were added and incubated for 2 h at RT with gentle orbital shaking. Plates were then washed 3 times with 150 µL PBS/well, incubated with 25 µL/well SULFOTAG Streptavidin (R32AD, Meso Scale Discovery) for 30 min at RT with gentle orbital shaking, then washed three times with 150 µL PBS/well. Finally, 150 µL/well of MSD GOLD Read Buffer B (R60AM, Meso Scale Discovery) were added and plates were read immediately on a MESO QuickPlex SQ 120 MM instrument. The following detection antibodies were used: CD63 Antibody, anti-mouse Biotin (clone REA563, Miltenyi Biotec); CD54 (ICAM-1) Antibody, anti-mouse, Biotin (clone YN1/1.7.4, #130-104-213, Miltenyi Biotec); CD86 Antibody, anti-mouse, Biotin (clone PO3.3, #130-101-944, Miltenyi Biotec); CD154 (CD40L) Antibody, anti-mouse, Biotin (clone MR1, #130-101-900, Miltenyi Biotec); H-2Kb/SIINFEKL Antibody, anti-mouse Biotin (clone 25-D1.16, Miltenyi Biotec).

9.3.2 | IL-12p70 Quantification by ECL Immunoassay

Il-12p70 was quantified using the V-PLEX Proinflammatory Panel 1 mouse kit (K152QVD, Meso Scale Discovery), following the manufacturer's assay protocol. Briefly, MULTI-SPOT 96-well plate pre-coated with capture antibodies was washed 3 times with 150 µL/well of wash buffer (R61AA, Meso Scale Discovery). Samples, calibrators, or controls (50 µL/well) were added, plates were sealed and incubated 2 h at room temperature (RT) with gentle orbital shaking. Plates were then washed 3 times with 150 µL/well of wash buffer, 25 µL/well of the SULFO-TAG–conjugated IL-12p70 detection antibody solution (D22QV, Meso Scale Discovery) was added, and plates were incubated 2 h at RT with gentle orbital shaking. After the final three washes with 150 µL/well of wash buffer, 150 µL/well of MSD GOLD Read Buffer B (R60AM, Meso Scale Discovery) were added and plates were read immediately on an a MESO QuickPlex SQ 120 MM instrument. Raw signals (ECL units) were converted to concentrations using the kit's calibration curve and analysed with the MSD software.

9.4 | OT-I T Cells Isolation and Activation

All animals were housed and handled at INSERM (mouse facility agreement number: #C67-482-33) according to the guidelines of INSERM and the ethical committee of Alsace (CREMEAS), following French and European Union animal welfare guidelines (Directive 2010/63/EU on the protection of animals used for scientific purposes). All procedures were performed in accordance with the ARRIVE guidelines, French and European Union animal welfare guidelines and supervised by local ethics committee. Animals were housed in pathogen-free conditions with food and water ad libitum and appropriate enrichment (sterile pulp paper and coarsely litter).

Single-cell suspensions of splenocytes were obtained by mechanical disruption of spleen from 8–12-week-old female wild-type C57BL/6-Tg (TcraTcrb)1100Mjb/Crl OT-I TCR transgenic mice (642OT1; Charles River) through a 30 µm nylon cell strainer (MiltenyiBiotec #1130-098-458). Red blood cells were lysed in ACK Buffer [150 mM NH_4Cl, 10 mM $KHCO_3$, 0.1 mM Na_2EDTA] for 3 min at room temperature. Naïve $CD8^+$ T cells were purified with a mouse Naïve $CD8a^+$ T cell Isolation Kit (MiltenyiBiotec #130-096-543). Purified naïve $CD8^+$ T cells purity was assessed by flow cytometry on a Attune NxT (Invitrogen) flow cytometer using FITC anti-CD4 (1:100, clone RM4-5, BioLegend #100510), BV605 anti-CD8 (1:200, clone 53–6.7, BioLegend #100743), PE anti-CD44 (1:200, clone IM7, BioLegend #103024), PE-Cy7 anti-TCR Va2 (1:100, clone B20.1, BioLegend #103024), and APC anti-TCR Vb5.1, 5.2 (1:100, clone MR9-4, BioLegend #139506) staining and ranged from 95.7 to 99.8 (median 99.3%).

Purified naïve $CD8^+$ T cells were then stained with 0.5 µM CellTrace Violet dye (Invitrogen #C34571) at 1×10^7 cells/ml in PBS for 15 min at 37°C in the dark before quenching with 1 vol ice-cold FCS for 5 min on ice. Labelled cells were washed, and 2×10^5 cells were treated with 5×10^9 EVs (i.e. $2{,}5 \times 10^4$ EVs/cell) at 37°C/5% CO_2 for 72 h in flat-bottomed 96 well plates in RPMI 1640 (Gibco #72400054) containing 2 mM Glutamine, 25 mM HEPES and completed with 10 % v/v of FBS (Gibco), 100 U/mL penicillin, 100 µg/mL streptomycin (PanBiotech #P06-07100) and 50 µM b-mercaptoethanol (Gibco #11508916). For positive control, 2×10^5 cells were cultured as above in wells previously coated with 5 µg/mL of anti-CD3e (clone 145-2C11, BioLegend #100301) and 5 µg/mL of anti-CD28 (clone 37.51, BioLegend #102101) in PBS overnight at 4°C. After incubation, the cells were washed in PBS and non-viable cells were stained with Fixable Viability Dye-eFluor780 (1:1,000, Invitrogen #L34993) for 15 min at room temperature in the dark. Then, cells were stained with PE anti-CD44 (1:200, clone IM7, BioLegend #103024) for 15 min at 4°C. Samples were acquired with Attune NxT (Invitrogen) flow cytometer and data were analysed using Kaluza Analysis Software 2.4 (Beckman Coulter).

9.5 | Mice and E.G7-OVA Tumor Model

All animals were housed and handled at the "Institut Clinique de la Souris" (mouse facility agreement number: #C67-218-40). All procedures experiments were approved by the local ethical committee (C2EA - 17 Comité d'éthique Com'Eth) for Animal Care and Use and research minister (APAFIS #40516 and #36730).

Female C57BL/6 and BALB/c mice 7 to 8 weeks of age were used for the experiments. The mice were purchased from Charles River and maintained in a temperature- and humidity-controlled animal facility (21 ± 2°C; 15%–70% humidity), with a 12-h light-dark cycle and free access to water and a standard rodent chow (D04, SAFE, Villemoisson-sur-Orge, France).

E.G7-OVA cells were subcutaneously injected at 3×10^5 cells per mouse in one abdominal flank. Therapeutic vaccines (1×10^7 PFU/mice) or EVs (9×10^8 to 4×10^9 EVs/mice) were injected intravenously 7 and 14 days after tumor inoculation. The size of superficial tumor was assessed three times per week by using a caliper and the body weight (BW) was monitored at the same

20013078, 2026, 6, Downloaded from https://isevjournals.onlinelibrary.wiley.com/doi/10.1002/jev2.70307 by Cochrane France, Wiley Online Library on [19/06/2026]. See the Terms and Conditions (https://onlinelibrary.wiley.com/terms-and-conditions) on Wiley Online Library for rules of use; OA articles are governed by the applicable Creative Commons License

time. Tumor volume was calculated with the spheroid formula V = (LxW^2)/2 after calculation of Width and Length diameter in the right angles. A maximal tumor volume of 2000 mm^3 and a maximum of 10% of BW loss between two measures have been considered as an ethical endpoint. Additional endpoint like ulceration, necrosis, and distension of covering tissues are recorded and would lead to terminate animals humanely when the degree of suffering cannot be justified by the scientific objective.

9.6 | Ex Vivo Studies / Pentamer SIINFEKL Staining

To detect and quantify $CD8^+$ OVA-specific T cells, a MHC-pentameric assay was used. Lymphocytes were isolated from heparinized blood taken at day D21 after tumor inoculation and incubated with 10 µL/test of R-PE Pro MHC Pentamer H-$2K^b$ SIINFEKL (#F093-2C-E, ProImmune) at +4°C for 30 min. Cells were resuspended and stained in wash buffer containing CD8a APC (1:50, clone 53–67, BD Pharmingen #553035) and CD19 V450 (1:50, clone 1D3, Tonbo biosciences #75-0193-U100) antibodies and incubated for 30 min at +4°C before flow cytometry analysis. The Pentamer-positive cells were viewed by gating first on CD19 negative lymphoid cells and then analysing on a two-color plot showing CD8 vs Pentamer. Samples were acquired with Aurora (Cytek) flow cytometer and data were analysed using SpectroFlo (Cytek) software.

9.7 | Cryo-electron Microscopy

Sample vitrification was performed using grids with a holey carbon film (Quantifoil R2/2) to which an additional continuous carbon support was added and which were previously cleaned for 1 min 30 in a Fischione 1070 plasma cleaner, in an 80% Argon/20% Oxygen gas mix. 3 µL of sample were applied on the grids, and excess of liquid was removed after 30s of incubation by blotting for 5s before vitrification by fast plunging in liquid ethane, using a Vitrobot Mark IV (Thermo Fisher Scientific) setup at 15°C and 95% humidity (Figure S1). Alternatively (Figure 1G), EVs were applied on previously glow discharged (Pelco EasiGlow) C-Flat copper grids 1.2/1.3 300 mesh (Electron Microscopy Sciences). Grids were then vitrified using a Vitrobot (ThermoFischer Scientific) in liquid ethane. The vitrification was performed at 4°C and 100% humidity, with a blotting time of 1 second. Grids were observed on the Glacios cryo-TEM (Thermo Fisher Scientific) operated at 200 kV, and images were recorded on K2 camera (Gatan) or with a Ceta-D camera, using EPU software with a pixel size of 1.9A/pixel and a total dose of about 20e/A2 per image.

9.8 | Statistical Analyses

Normality was determined using a Shapiro-Wilk test. Unpaired t test was used for paired comparison data following a normal distribution and Mann-Whitney test otherwise. Multiple comparison was analysed using a one-way anova or a two-way anova test for data following a normal distribution or a Kruskal-Wallis test otherwise.

10 | Results

10.1 | Size Filtration Allows the Separation of sEVS From Infectious Viral Particles

Aiming at analysing the immunomodulatory potential of EVs secreted by cells infected with immunotherapeutic poxviruses, we first investigated which isolation method would reliably separate them from viral particles. This step is challenging, as poxviruses are dsDNA enveloped viruses, approximately 200–300 nm in diameter (McInnes et al. 2023), that share size, structural and biophysical characteristics with EVs (Nolte-'t Hoen et al. 2016; Cortes-Galvez et al. 2023). In order to selectively isolate EVs from infectious viral particles, which is mandatory for their analysis and further use, we compared some of the most classical and robust EV isolation methods: UC, immunocapture, density gradient, velocity gradient, size exclusion chromatography (SEC) and filtration (Figure 1A and S1A–C) (Welsh et al. 2024). PBMCs from healthy donors were infected with a typical representative of the Poxviridae family (of which other versions are currently tested in therapy, ClinicalTrials.gov identifier NCT04725331): the VV_{COP}, encoding eGFP reporter protein (VV_{COP}-eGFP). Cells were infected at a multiplicity of infection of 1 (MOI = 1) over night and secreted EVs (and other co-isolated particles, including remaining or newly-secreted viral particles) were isolated, measured and quantified by nanoparticle tracking analysis (NTA). The presence of residual infectious viral particles was probed by titration of plaque forming units (PFU).

We first observed that UC at 100,000 g co-pelleted both EVs and infectious viral particles (Figure 1B). In order to visualize EVs, we performed electron microscopy and confirmed that such method cannot separate EVs from brick-shaped viral particles that have overlapping size and density (Figure S1A). We next tested a method relying on the immunocapture of tetraspanins (CD9, CD81 and CD63), which are classically present on the surface of EVs (Welsh et al. 2024). While this approach efficiently captured high amounts of particles, it also retained most of the infectivity present in the samples (Figure 1C). This may be explained by the fact that poxviruses, particularly in their enveloped form, known as extracellular enveloped virus (EEV), originate at least in part from tetraspanin-rich compartments, such as multivesicular bodies (MVB) (Huttunen et al. 2021) and incorporate host cell components in their envelop (Vanderplasschen et al. 1998).

We then tested fractionation methods based on the structural properties of the particles, hoping to identify fractions containing EVs and deprived of infectious particles. To this end, we tried to separate EVs from viral particles based on their density, using an iodixanol density gradient. The most infectious fractions (fractions 10–15) were distinctly separated from the fractions enriched in particles (fractions 1–4 and fractions 8–10) (Figure 1D). Interestingly, viral infection is associated with the apparition of low-density particles (fractions 1–4) distinct from usual EV fractions (fractions 8–10) (Figure S2C) which could correspond to previously described EVs-virus intermediates (Nolte-'t Hoen et al. 2016). Yet, infectious viral particles were identified in each of the 17 fractions collected, thereby excluding density gradient centrifugation as an efficient method to separate EVs from viral particles. We next used velocity

20013078, 2026, 6, Downloaded from https://isevjournals.onlinelibrary.wiley.com/doi/10.1002/jev2.70307 by Cochrane France, Wiley Online Library on [19/06/2026]. See the Terms and Conditions (https://onlinelibrary.wiley.com/terms-and-conditions) on Wiley Online Library for rules of use; OA articles are governed by the applicable Creative Commons License

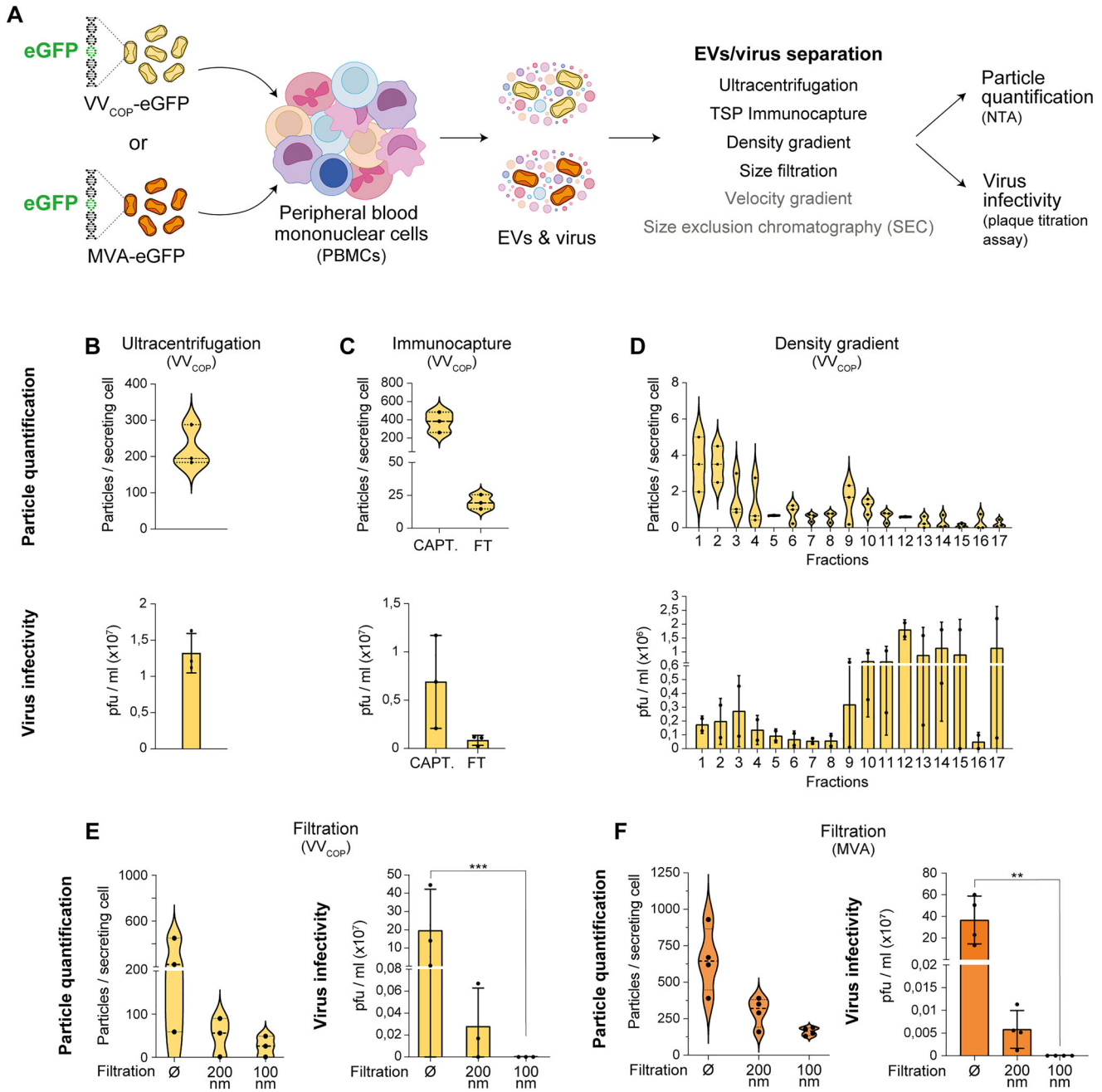


FIGURE 1 | : 100 nm filtration allows to efficiently separate small EVs from infectious poxvirus particles. A) Workflow for the comparison of six different EV isolation methods tested for their ability to separate small EVs from infectious poxvirus particles from the supernatant of human peripheral blood mononuclear cells (PBMCs) infected by VVCOP (B–E) or MVA (F) poxvirus at a multiplicity of infection of 1 (MOI = 1). Particles were quantified by NTA and virus infectivity was assessed by titration of plaque forming units (PFU). B–F) Top: quantification of the number of isolated particles per secreting cell; Bottom: quantification of the virus infectivity. Supernatants from poxvirus-infected PBMCs were processed by ultracentrifugation (B), $N = 3$ independent experiments; pan-tetraspanin immunocapture (C) (CAPT.: captured particles; FT: flow through), $N = 3$ independent experiments; iodixanol density gradient (D), $N = 3$ independent experiments; and filtration (E–F) at 200 nm (0.2 μm) or 100 nm (0.1 μm) followed by ultracentrifugation, $N = 3$ independent experiments for VVCOP in (E), Filtered 100 nm $p = 0{,}019$, Kruskal-Wallis; and $N = 4$ independent experiments for MVA in (F), Filtered 100 nm $p = 0{,}0028$, Kruskal-Wallis. ** $p < 0{,}05$; *** $p < 0{,}005$.

gradient, which was recently shown to segregate HIV virus from small vesicles 2009(Martin-Jaular et al., 2021), and size-based fractionation using size-exclusion chromatography (Figure S1B–C). These methods equally failed to separate infectious poxvirus particles from EVs, demonstrating that neither size- nor density-based methods fractionation can efficiently overcome the shared characteristics of poxvirus particles and EVs. Finally, we investigated whether a size cut-off filtration (*i.e.* positive enrichment of small sized particles) could efficiently separate sEVs from viral particles. To test this approach, we applied 200 nm or 100 nm filtration followed by UC (Figure 1E–F). While 200 nm filtration significantly reduced the viral load (around a thousand-

20013078, 2026, 6, Downloaded from https://isevjournals.onlinelibrary.wiley.com/doi/10.1002/jev2.70307 by Cochrane France, Wiley Online Library on [19/06/2026]. See the Terms and Conditions (https://onlinelibrary.wiley.com/terms-and-conditions) on Wiley Online Library for rules of use; OA articles are governed by the applicable Creative Commons License

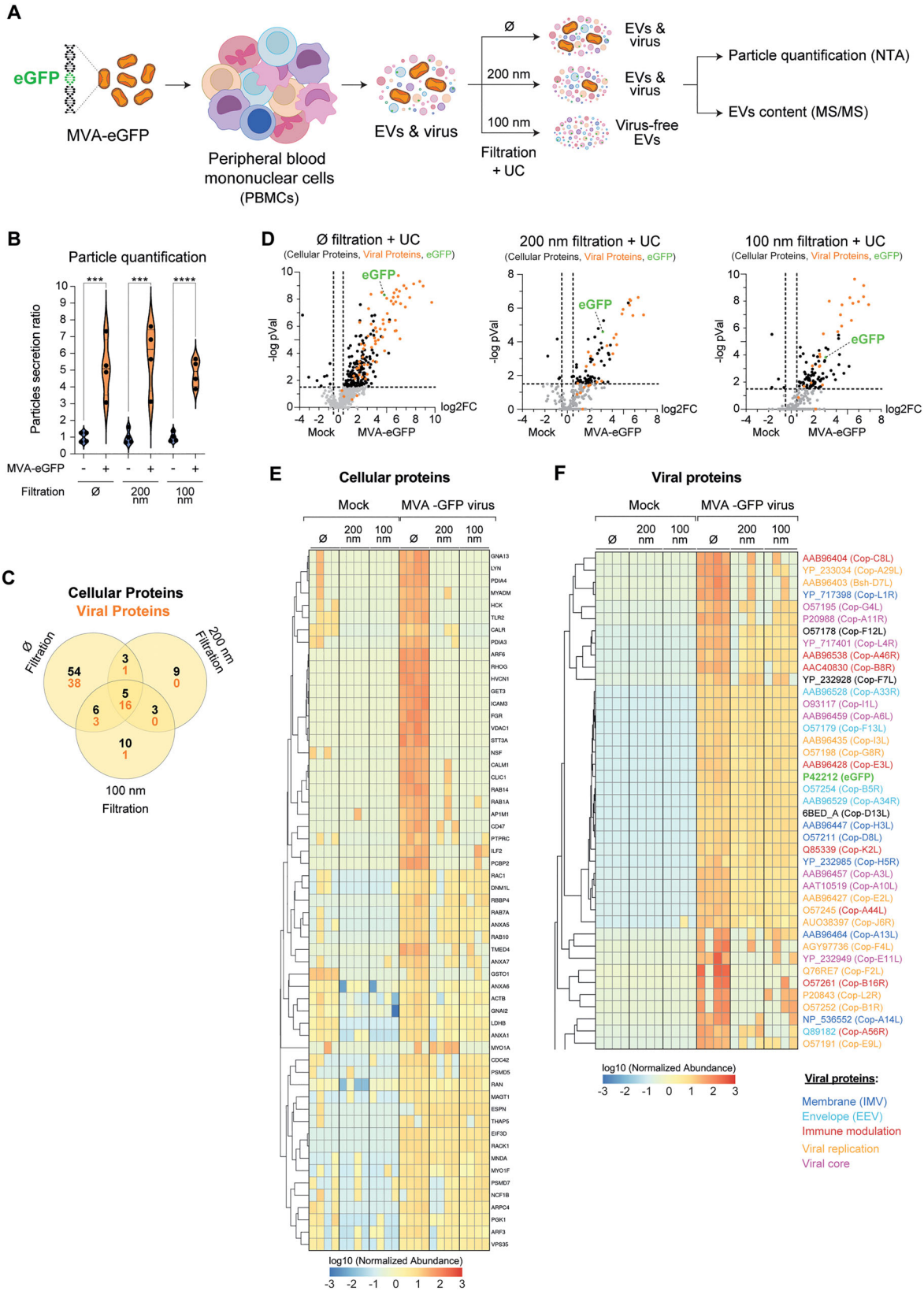


FIGURE 2 | : MVA infection increases the secretion of small EVs with distinct protein content. A) EVs secreted by human peripheral blood mononuclear cells (PBMC) infected by eGFP-MVA poxvirus were isolated by ultracentrifugation after 100 nm or 200 nm filtration, quantified by NTA (B) and their content was characterized by mass spectrometry (C–F). B) Quantification by NTA of the number of particles per secreting cell in non-infected mock (blue) and MVA-infected (orange) conditions with and without filtration (normalized to mock). $N = 4$ independent experiments. Unfiltered $p =$ 0,0034; Filtered 200 nm $p = 0{,}003$; Filtered 100 nm $p = 0{,}0001$, Unpaired T-test. C) Venn diagram showing viral (orange) and cellular (black) proteins

20013078, 2026, 6, Downloaded from https://isevjournals.onlinelibrary.wiley.com/doi/10.1002/jev2.70307 by Cochrane France, Wiley Online Library on [19/06/2026]. See the Terms and Conditions (https://onlinelibrary.wiley.com/terms-and-conditions) on Wiley Online Library for rules of use; OA articles are governed by the applicable Creative Commons License

fold), it failed to provide a purified particle preparation devoid of infectivity. In contrast, 100 nm filtration successfully yielded virus-free sEVs, with a diameter of approximately 130–150 nm as measured by NTA (Figure 1E). Extending this approach to MVA, another widely used and well-characterised vaccinia virus strain, we showed it equally succeed in isolating sEVs free of infectious particles (Figure 1F). However, such method remained inefficient to separate sEVs from the PCPV (*Parapoxvirus*), which appears more elongated than the brick-shaped VV_{COP} and MVA (*Orthopoxvirus*) as previously described (Gelderblom et Madeley 2018) and might therefore not be fully retained by 100 nm pores (Figure S1D–E). Altogether, this careful screen of particle isolation methods demonstrates that 100 nm filtration coupled to UC (or to other isolation methods, such as SEC) is the only one efficiently segregating sEVs from any VV_{COP} and MVA infectious viral particles while allowing to collect sufficient amounts of virus-free sEVs. This protocol now allows for the first time to investigate the immunomodulatory potential specific to sEVs secreted by orthopoxvirus-infected cells.

10.2 | MVA Infection Enhances EVs Secretion by PBMCs and Alters Their Content

Building on a reliable method to study sEVs from infected cells, we then investigated the impact of poxvirus infection on EV secretion levels and content (Figure 2A). In our subsequent work we focused on the attenuated *Orthopoxvirus* strain MVA since this virus maintains a strong immunogenicity profile and serves as the backbone for MVA-based vectors currently under clinical evaluation as therapeutic cancer vaccine. PBMCs from healthy donors were infected with MVA-eGFP, allowing to track virus-encoded payload and EVs deprived of infectious viral particles were isolated by UC combined with 100 nm filtration and quantified by NTA. We found that MVA infection leads to a five-fold increase in the number of sEVs compared to a non-infected condition (Figure 2B). Such increase was observed independently of the isolation method (UC (Figure S2A), density (Figure S2C) or velocity gradient (Figure S2D), and SEC (Figure S2E)) and the poxviruses strain tested (Figure S2F), suggesting that poxvirus-infected PBMCs significantly increase their EV secretion levels. We next wondered whether the infection had any impact their content. Mass spectrometry analyses of EVs from poxvirus-infected PBMCs revealed that MVA-eGFP infection markedly alters the protein composition of sEVs (Figure 2C–F, Figure S3). GO terms analysis of the differentially expressed proteins revealed an enrichment for terms associated with EVs, host-virus interactions and adaptative immunity (Figure S3A). Around 50 PBMCs cellular proteins displayed a differential expression, most of them showing an increase post-infection (Figure 2C–E; Tables 1-3). Among them, we found proteins related to viral response (SAMHD1, Rack1, Magt1), translation (RPL5, EIF3D, RPS9), vesicular trafficking (Rab7, VPS35) and actin polymerization (Espin, Arpc4, Profilin, Myo1A). In addition, we identified various viral proteins associated with EVs upon the different filtration methods. While their presence in the unfiltered samples could be explained by the co-isolation of viral particles (Figure 2C, D, F, Figure S3B, Table 1), their presence after the 100 nm filtration reveals that some viral proteins are integrated at the surface or inside sEVs secreted after infection (Figure 2C, D, F, **Table** 3). Among them, we identified core viral proteins, membrane and envelope proteins as well as proteins involved in viral replication and in immune modulation (Figure 2F). Notably, we also observed the presence of virus-encoded eGFP in sEVs after 100 nm filtration (Figure 2D, F). Overall, we show that poxvirus (MVA) infection not only stimulates EV secretion in infected cells, but also significantly modifies their content, with upregulation of cellular proteins associated with viral infection and replication, as well as incorporation of various viral proteins. Most importantly, we demonstrated that exogenous payloads encoded by the virus (eGFP) can be efficiently transferred to sEVs secreted by infected cells, which opens the door to studying the transfer of immunomodulatory payloads to EVs, as a mean to leverage the therapeutic effect of the viral vector.

10.3 | Dendritic Cell–Derived EVs Carry Therapeutic Payloads Encoded by an Armed MVA

Prompted by the observation that virus-encoded eGFP can be transferred to sEVs, we next investigated whether therapeutic virus-encoded immunomodulatory payloads could be similarly transferred. In order to investigate payloads with proven immune-modulatory antitumor efficacy, we exploited the E.G7-OVA mouse lymphoma model to first compare the efficacy of various versions of therapeutic MVA vectors (Figure S4). Our results demonstrate that the highest anti-tumoral efficacy is obtained when several payloads were combined into one armed MVA: (i) two epitopes of ovalbumin (OVA) as model antigens, including the widely used MHC class I-presented strong SIINFEKL peptide agonist to elicit OVA-specific responses, together with (ii) the soluble murine cytokine IL-12, endogenously secreted by mature antigen-presenting cells (APC) to promote $CD8^+$ T cells differentiation into effector cytotoxic T lymphocytes (Mirlekar and Pylayeva-Gupta, 2021), and iii) the murine CD40L, a membrane-bound immunostimulatory molecule which binds to CD40 to promote DC maturation, cytokines production, and prime $CD8^+$ T cell into cytotoxic T cells (Elgueta et al. 2009). Interestingly, both IL12 and CD40L independently improve poxvirus-induced antitumor immune response in mice models(Medina-Echeverz et al. 2019; Bella et al. 2023) (and Figure S4). Given its greater antitumor effect compared to single or double armed virus

identified in ultracentrifugation pellet, with or without filtration (100 nm or 200 nm). D) Volcano plots showing viral (orange) and cellular (black) proteins identified in EVs isolated by ultracentrifugation, with or without filtration (100 nm or 200 nm) and differentially expressed between non-infected mock and MVA-infected conditions. Proteins with a p-value < 0,01 and a log2FC > 0,5 were considered. Virus-encoded eGFP is highlighted in green. E–F) Heat map showing the normalized abundance of cellular (E) viral (F) proteins identified in ultracentrifugation pellet with or without filtration (100 nm or 200 nm) and color-coded by functional category. Label corresponds to MVA Uniprot ID (VVcop ortholog). Values are displayed as log10-transformed, normalized and centered by gene, with the corresponding color scale shown in the legend below. For proteins undetected by mass spectrometry in a given condition, the value was arbitrarily set to 0. Mass spectrometry was performed in quadruplicate. *** $p < 0{,}005$; **** $p < 0{,}001$.

20013078, 2026, 6, Downloaded from https://isevjournals.onlinelibrary.wiley.com/doi/10.1002/jev2.70307 by Cochrane France, Wiley Online Library on [19/06/2026]. See the Terms and Conditions (https://onlinelibrary.wiley.com/terms-and-conditions) on Wiley Online Library for rules of use; OA articles are governed by the applicable Creative Commons License

TABLE 1 | Mass spectrometry on EVs isolated by ultracentrifugation.

ID	protein_set_id	Origin	logFC	P_Value
ORF201|AAT10519	47600	Viral (MVA)	9,665442413	1,67925E-08
ORF188|AAB96457	47770	Viral (MVA)	8,78336799	1,05529E-09
ORF65|O57179	48279	Viral (MVA)	8,433699263	4,7812E-10
ORF171|O57211	47286	Viral (MVA)	7,803188882	7,32805E-10
ORF130|YP_717401	47638	Viral (MVA)	7,390988621	7,46922E-09
ORF182|6BED_A	50908	Viral (MVA)	7,036138521	1,56367E-09
ORF98|O93117	49813	Viral (MVA)	6,932340822	3,75336E-08
ORF145|AAB96447	48599	Viral (MVA)	6,782278721	9,79293E-10
ORF81|AAB96487	47902	Viral (MVA)	6,443573382	2,10861E-08
ORF140|AUO38397	49444	Viral (MVA)	6,393241235	8,57386E-06
ORF190|AAB96458	48413	Viral (MVA)	6,328162538	2,54838E-09
ORF288|O57254	47647	Viral (MVA)	6,214372309	1,75143E-10
ORF241|AAB96529	47790	Viral (MVA)	6,173384081	6,34796E-09
ORF194|AAB96459	48263	Viral (MVA)	6,011744561	1,93156E-09
ORF146|O57207	48146	Viral (MVA)	5,987889652	2,07898E-06
ORF260|O57245	47345	Viral (MVA)	5,946945456	1,53739E-08
ORF155|O57209	47566	Viral (MVA)	5,913085223	3,59157E-07
ORF226|QCI57162	47370	Viral (MVA)	5,874802718	2,2127E-06
ORF70|YP_717364	48048	Viral (MVA)	5,765116219	3,29533E-09
ORF128|AAS49792	49474	Viral (MVA)	5,698264308	2,23756E-08
ORF101|AAB96435	48160	Viral (MVA)	5,684980208	7,12774E-09
ORF240|AAB96528	47718	Viral (MVA)	5,469182385	1,35043E-08
sp|P63243|RACK1_BOVIN	49348	Cellular	5,308682002	3,31679E-07
ORF121|YP_232967	47016	Viral (MVA)	5,266196097	4,56309E-07
sp|O00160|MYO1F_HUMAN	50154	Cellular	5,212868987	9,69953E-05
ORF196|O57220	47439	Viral (MVA)	5,067759317	1,12582E-07
ORF136|YP_232977	48012	Viral (MVA)	5,010356072	8,55054E-09
ORF114|P68492	47831	Viral (MVA)	4,831066629	1,71674E-06
ORF110|AAB96439	48210	Viral (MVA)	4,796356226	6,47847E-05
CON_sp|P42212|GFP_AEQVI	48779	Viral (MVA)	4,771546517	4,77733E-09
ORF124|O57198	47343	Viral (MVA)	4,648059912	6,48325E-07
ORF74|AAB96427	47459	Viral (MVA)	4,633871877	3,27779E-07
ORF262|AAB96538	49225	Viral (MVA)	4,585878782	6,24606E-06
ORF112|O57193	48470	Viral (MVA)	4,482241782	3,09617E-09
sp|Q93070|NAR4_HUMAN	47481	Cellular	4,442432015	5,65967E-06
ORF293|AAC40830	48699	Viral (MVA)	4,334237605	1,56767E-06
ORF77|AAB96428	47022	Viral (MVA)	4,139406641	1,00829E-05
sp|P09203|TBB1_CHICK	50854	Cellular	4,004177996	0,000137106
ORF167|O93120	47173	Viral (MVA)	3,966894798	0,000433629
ORF205|P20988	47477	Viral (MVA)	3,960324706	2,50872E-06
sp|P51149|RAB7A_HUMAN	49250	Cellular	3,884593187	0,000429064

(Continues)

20013078, 2026, 6, Downloaded from https://isevjournals.onlinelibrary.wiley.com/doi/10.1002/jev2.70307 by Cochrane France, Wiley Online Library on [19/06/2026]. See the Terms and Conditions (https://onlinelibrary.wiley.com/terms-and-conditions) on Wiley Online Library for rules of use; OA articles are governed by the applicable Creative Commons License

TABLE 1 | (Continued)

ID	protein_set_id	Origin	logFC	P_Value
ORF175|O57214	47442	Viral (MVA)	3,848028289	1,98334E-05
ORF234|YP_233034	49373	Viral (MVA)	3,846383232	1,36378E-06
ORF55|YP_232928	47866	Viral (MVA)	3,844548766	1,21949E-05
ORF85|AAB96489	47114	Viral (MVA)	3,841543893	1,28304E-06
sp|P04839|CY24B_HUMAN	50490	Cellular	3,832539465	0,005283716
sp|P22451|RL5_CHICK	48453	Cellular	3,771088416	1,50155E-07
ORF163|AAB96514	47296	Viral (MVA)	3,757246485	7,19448E-06
sp|B5ME19|EIFCL_HUMAN	48231	Cellular	3,676497797	4,593E-06
CON_sp|P08758|ANXA5_HUMAN	48763	Cellular	3,634526593	0,002166703
sp|P62191|PRS4_HUMAN	49854	Cellular	3,632919887	4,19687E-07
sp|A6QLG5|RS9_BOVIN	47225	Cellular	3,629966203	2,04084E-06
sp|P08575|PTPRC_HUMAN	49772	Cellular	3,626473657	0,002365265
sp|O60603|TLR2_HUMAN	50862	human	3,617782095	9,42358E-05
ORF208|NP_536552	46918	Viral (MVA)	3,6026382	0,000367176
sp|P41218|MNDA_HUMAN	48032	human	3,497689122	5,66611E-05
sp|P62269|RS18_HUMAN	49458	Cellular	3,467864573	1,69824E-07
ORF30|Q85339	50137	Viral (MVA)	3,441075587	3,66301E-05
ORF126|YP_717398	47889	Viral (MVA)	3,402388774	6,82038E-07
ORF63|O57178	48073	Viral (MVA)	3,384938367	4,26424E-09
sp|P02771|FETA_HUMAN	48748	Cellular	3,365382739	0,000656744
sp|P62194|PRS8_BOVIN	49853	Cellular	3,359005092	3,8089E-06
CON_sp|P61626|LYSC_HUMAN	47500	Cellular	3,292315347	0,000252846
sp|Q9Y3Z3|SAMH1_HUMAN	48298	Cellular	3,279382477	0,001115545
sp|P11940|PABP1_HUMAN	49491	Cellular	3,266002414	0,000176799
ORF35|AAB96411	47660	Viral (MVA)	3,129021463	4,94158E-08
sp|Q15907|RB11B_HUMAN	49764	Cellular	3,11244976	0,000482508
ORF58|O57177	46944	Viral (MVA)	3,073546105	5,40269E-06
sp|P01903|DRA_HUMAN	50277	Cellular	3,069005246	0,009051433
ORF87|O57191	48027	Viral (MVA)	3,039851996	0,000689547
ORF276|Q89182	47084	Viral (MVA)	2,992614017	0,003511872
sp|P68371|TBB4B_HUMAN	50850	Cellular	2,938067055	0,000191844
sp|P61106|RAB14_HUMAN	50824	Cellular	2,893574469	6,96964E-06
sp|P35998|PRS7_HUMAN	49136	Cellular	2,864100338	0,00034937
sp|P30740|ILEU_HUMAN	50503	Cellular	2,85446744	0,003397104
ORF149|YP_232985	49495	Viral (MVA)	2,825437895	0,007614978
sp|P25789|PSA4_HUMAN	48408	Cellular	2,731347614	5,54232E-05
ORF216|AAB96468	47772	Viral (MVA)	2,725815609	2,50098E-05
sp|P08195|4F2_HUMAN	47585	Cellular	2,709501352	0,000251707
sp|P62244|RS15A_HUMAN	49425	Cellular	2,699718475	0,00597512
sp|P62280|RS11_HUMAN	48082	Cellular	2,689509856	0,002758257
sp|P42558|RAN_CHICK	48962	Cellular	2,679850258	0,002796113

(Continues)

20013078, 2026, 6, Downloaded from https://isevjournals.onlinelibrary.wiley.com/doi/10.1002/jev2.70307 by Cochrane France, Wiley Online Library on [19/06/2026]. See the Terms and Conditions (https://onlinelibrary.wiley.com/terms-and-conditions) on Wiley Online Library for rules of use; OA articles are governed by the applicable Creative Commons License

TABLE 1 | (Continued)

ID	protein_set_id	Origin	logFC	P_Value
ORF132|AAB96502	48618	Viral (MVA)	2,677293782	0,000684737
sp|P20073|ANXA7_HUMAN	48756	Cellular	2,667683119	0,000552404
ORF179|O57215	49231	Viral (MVA)	2,65039789	0,002970238
sp|P60842|IF4A1_HUMAN	48908	Cellular	2,610704497	0,001338692
ORF158|AUO38407	48276	Viral (MVA)	2,607720974	4,5887E-05
sp|A4FUD3|U5S1_BOVIN	50368	Cellular	2,600339811	0,002800792
sp|O00429|DNM1L_HUMAN	48650	Cellular	2,598648213	0,003904439
sp|P63151|2ABA_HUMAN	50402	Cellular	2,59426181	1,75148E-05
sp|P07948|LYN_HUMAN	50845	Cellular	2,582186953	0,00541684
sp|P61026|RAB10_HUMAN	50821	Cellular	2,574114694	0,000121481
sp|P05107|ITB2_HUMAN	49866	Cellular	2,559721453	0,007691473
ORF72|O57184	47147	Viral (MVA)	2,532660851	0,000188383
sp|P62913|RL11_HUMAN	48619	Cellular	2,51934644	1,13229E-05
sp|P62333|PRS10_HUMAN	50302	Cellular	2,516998566	0,000489413
sp|P46459|NSF_HUMAN	51264	Cellular	2,503404061	0,001429662
sp|Q15366|PCBP2_HUMAN	49950	Cellular	2,478559548	0,000229264
ORF143|P07239	47485	Viral (MVA)	2,47414261	0,005712331
sp|P11017|GBB2_BOVIN	51056	Cellular	2,465527544	7,75872E-05
sp|P61204|ARF3_HUMAN	50177	Cellular	2,457534671	0,000160318
sp|P33176|KINH_HUMAN	51394	Cellular	2,451327422	0,001251541
sp|P46977|STT3A_HUMAN	49927	Cellular	2,438726583	0,001418565
sp|Q96JB1|DYH8_HUMAN	48113	Cellular	2,422540169	0,000936827
sp|P55072|TERA_HUMAN	48790	Cellular	2,388888991	0,000984091
sp|P30101|PDIA3_HUMAN	49623	Cellular	2,375615895	0,001318566
ORF117|O57195	49300	Viral (MVA)	2,374702214	2,04073E-05
sp|O15371|EIF3D_HUMAN	48101	Cellular	2,353874184	4,65215E-06
sp|P51665|PSMD7_HUMAN	50578	Cellular	2,326881493	0,000409518
sp|Q7Z7H5|TMED4_HUMAN	47834	Cellular	2,302087928	0,000615412
sp|P38919|IF4A3_HUMAN	48909	Cellular	2,301088124	0,001719965
sp|P60953|CDC42_HUMAN	50006	Cellular	2,295839961	0,000391052
sp|P48463|PP2AA_CHICK	49708	Cellular	2,284983561	2,49657E-08
sp|P46940|IQGA1_HUMAN	49984	Cellular	2,273257476	0,002392034
sp|P52566|GDIR2_HUMAN	50250	Cellular	2,251183623	5,39445E-06
sp|P62820|RAB1A_HUMAN	50820	Cellular	2,230814597	3,82449E-07
ORF137|AUO38395	47480	Viral (MVA)	2,221747494	0,000745824
ORF217|O57227	47024	Viral (MVA)	2,207200869	5,06322E-07
sp|O13268|PSA7_CHICK	51334	Cellular	2,191275772	0,00259618
ORF270|O57250	46933	Viral (MVA)	2,188560859	0,000408699
ORF160|AUO38406	47711	Viral (MVA)	2,172590652	0,003887747
sp|P08631|HCK_HUMAN	50843	Cellular	2,164782389	2,16724E-05
sp|P13667|PDIA4_HUMAN	47535	Cellular	2,157506331	0,001487578
ORF23|AAB96404	47338	Viral (MVA)	2,119741916	0,001182847
sp|P13498|CY24A_HUMAN	48664	Cellular	2,06284305	0,006995338

(Continues)

20013078, 2026, 6, Downloaded from https://isevjournals.onlinelibrary.wiley.com/doi/10.1002/jev2.70307 by Cochrane France, Wiley Online Library on [19/06/2026]. See the Terms and Conditions (https://onlinelibrary.wiley.com/terms-and-conditions) on Wiley Online Library for rules of use; OA articles are governed by the applicable Creative Commons License

TABLE 1 | (Continued)

ID	protein_set_id	Origin	logFC	P_Value
sp|P04083|ANXA1_HUMAN	50069	Cellular	2,045492592	0,008050547
sp|P25786|PSA1_HUMAN	48517	Cellular	2,029537444	0,004987858
sp|P61763|STXB1_BOVIN	49564	Cellular	2,015226284	0,00167707
sp|O00299|CLIC1_HUMAN	49119	Cellular	2,014087991	0,00678117
sp|P26990|ARF6_CHICK	47708	Cellular	1,973817995	6,86631E-05
sp|O00487|PSDE_HUMAN	49340	Cellular	1,972103007	0,000600852
sp|P39656|OST48_HUMAN	48132	Cellular	1,936543271	0,00038002
ORF8|AAB96403	47496	Viral (MVA)	1,910491014	0,001341962
sp|P50990|TCPQ_HUMAN	51020	Cellular	1,900824838	0,001080302
sp|P11021|BIP_HUMAN	51134	Cellular	1,888230656	0,00112853
sp|P17858|PFKAL_HUMAN	51375	Cellular	1,876711708	0,004034929
sp|P27797|CALR_HUMAN	50685	Cellular	1,840584573	0,003838779
sp|Q29466|VPP1_BOVIN	49287	Cellular	1,832390982	5,22583E-06
sp|Q6P4A8|PLBL1_HUMAN	48098	Cellular	1,789804605	0,004750862
sp|P84095|RHOG_HUMAN	48692	Cellular	1,777799859	0,000518878
sp|P09960|LKHA4_HUMAN	49189	Cellular	1,737145887	0,005089934
sp|P51659|DHB4_HUMAN	50767	Cellular	1,732547773	0,000637858
ORF206|O57224	49359	Viral (MVA)	1,710192362	0,007384562
sp|P62888|RL30_HUMAN	48653	Cellular	1,687646093	0,006583043
sp|P62998|RAC1_BOVIN	49202	Cellular	1,6604938	0,003009035
sp|Q02543|RL18A_HUMAN	51248	Cellular	1,635092296	0,000511842
ORF28|AAB96408	47323	Viral (MVA)	1,595679222	0,004598653
sp|P14314|GLU2B_HUMAN	49091	Cellular	1,583783692	0,003741943
sp|Q13488|VPP3_HUMAN	49128	Cellular	1,563007226	0,00109709
sp|Q09028|RBBP4_HUMAN	49229	Cellular	1,558773005	0,003089604
sp|P0DP23|CALM1_HUMAN	49553	Cellular	1,476465962	0,001869951
sp|Q14344|GNA13_HUMAN	51258	Cellular	1,43208902	0,004306998
sp|Q96S97|MYADM_HUMAN	47670	Cellular	1,403844478	0,005644634
sp|P35080|PROF2_HUMAN	49646	Cellular	1,392783389	0,00016641
sp|Q08722|CD47_HUMAN	50712	Cellular	1,313552484	0,002432588
sp|P21796|VDAC1_HUMAN	48049	Cellular	1,298234461	0,005411392
sp|P32942|ICAM3_HUMAN	47306	Cellular	1,287621316	0,002745214
sp|P00491|PNPH_HUMAN	49569	Cellular	1,279370591	0,004555363
sp|P09769|FGR_HUMAN	50841	Cellular	1,273127917	0,009260736
sp|Q12905|ILF2_HUMAN	49547	Cellular	1,25327027	0,000562588
sp|P25705|ATPA_HUMAN	51222	Cellular	1,251593437	2,70868E-05
sp|P25774|CATS_HUMAN	48379	Cellular	1,232785164	0,004622936
sp|Q9H4G4|GAPR1_HUMAN	48547	Cellular	1,227810419	0,003190192
sp|P57088|TMM33_HUMAN	49527	Cellular	1,171972661	0,000901659
sp|A5PJI5|GET3_BOVIN	49439	Cellular	1,132038167	0,000182734
sp|Q2KJ81|AP1M1_BOVIN	50526	Cellular	1,117888663	0,004983378
sp|A6QLP7|SSRA_BOVIN	49145	Cellular	1,068789193	4,13127E-05
sp|Q96D96|HVCN1_HUMAN	51261	Cellular	1,053707626	0,009929016

(Continues)

20013078, 2026, 6, Downloaded from https://isevjournals.onlinelibrary.wiley.com/doi/10.1002/jev2.70307 by Cochrane France, Wiley Online Library on [19/06/2026]. See the Terms and Conditions (https://onlinelibrary.wiley.com/terms-and-conditions) on Wiley Online Library for rules of use; OA articles are governed by the applicable Creative Commons License

TABLE 1 | (Continued)

ID	protein_set_id	Origin	logFC	P_Value
sp|P08133|ANXA6_HUMAN	50465	Cellular	1,00910349	0,00210974
sp|Q10471|GALT2_HUMAN	48597	Cellular	1,007754108	0,009588183
sp|P46783|RS10_HUMAN	49011	Cellular	0,959665145	0,003437426
sp|P62326|TYB4_BOVIN	50534	Cellular	−0,851233464	0,000571768
sp|P42229|STA5A_HUMAN	49946	Cellular	−1,180963102	0,004536449
sp|P78417|GSTO1_HUMAN	49641	Cellular	−1,437875859	0,005112945
sp|P02272|H2AV_CHICK	51168	Cellular	−3,064984385	0,005819296
sp|Q9NWT1|PK1IP_HUMAN	49750	Cellular	−3,704658952	1,48014E-07

Note: Proteins differentially expressed between mock and MVA infected PBMCs are shown (p-value < 0,01). Positive log fold change (logFc): increased expression post-infection. Negative log fold change (logFc): decreased expression post-infection. Chick peptides might originate from initial viral production in chicken embryo fibroblast. Data presented on Figure 2 and Supplementary Figure 3.

(Figure S4), we selected the triple-armed vector to study how it impacts the content and function of EVs released post-infection. In addition, the triple-armed vector offers the possibility to study payloads with complementary localizations, since IL–12 is supposed to be secreted whereas CD40L and SIINFEKL presented by murine MHC-I (H-2K^b) upon intracellular processing should be membrane bound, allowing us to track their association with sEVs. For testing the immunomodulatory potential of sEVs upon viral infection, we targeted professional antigen-presenting DC, as DC-derived EVs are known for their ability to present co-stimulatory molecules and antigen/MHC complexes on their surface that are able to trigger T cells response (Schioppa et al. 2024). More importantly, DC are well infected by MVA vector (Liu et al. 2008) and DC-derived EVs can elicit specific anti-tumor immune responses (Matsumoto et al. 2020). To explore this potential, we opted for the murine dendritic cell line DC2.4 (Liu et al. 2022), which was established from a C57BL/6 background and thus compatible with our E.G7-OVA model. After infection with either the triple-armed MVA (^{armed}MVA) or an empty MVA (^{empty}MVA), sEVs were isolated from infected DC (iDC) by 100 nm filtration followed by UC, as previously described, yielding ^{armed}iDC-EVs-UC and ^{empty}iDC-EVs-UC, respectively. sEVs from non-infected cells processed identically served as controls (DC-EVs-UC). In addition, we replaced UC with SEC after the 100 nm filtration, to further refine the separation (Sidhom et al. 2020; Soares et al. 2023) of sEVs (^{armed}iDC-EVs-SEC) from soluble proteins (^{armed}iDC-Prots-SEC) (Figure 3A). EVs isolated by UC or SEC post-100 nm filtration do not contain mature virions, as expected, but heterogenous internal electron dense structures (Cryo-electron microscopy, Figure 3B). To characterise the surface composition of these various sEVs we used an ELISA-like chemiluminescence immunoassay. Looking at markers of cellular origins, we observed reduced levels of the tetraspanin CD63, closely associated with endosomal-derived vesicles (Pols and Klumperman, 2009), at the surface of sEVs from infected DC2.4, independently of whether the virus was armed or not and independently of the EV isolation method (Figure 3C). We also analysed two immunomodulatory proteins whose presence at the surface of DC promotes T cells activation: ICAM1 and CD86. ICAM1 is known for its important role in immune synapse strengthening by binding to LFA-1 (Bromley and Dustin, 2002; Sapoznikov et al. 2023; Zhou et al. 2025), allowing the stabilisation of the interaction between DC-derived EVs and T cells (Nolte-'t Hoen et al. 2009) and it has been shown that its addition to the surface of engineered-EVs enhances mouse CD4$^+$ and CD8$^+$ T cell activation (Segura et al. 2005; Lyu et al. 2025). CD86 is a key co-stimulatory molecule involved in T cell activation through its interaction with CD28 (Thomas et al. 2007). EV surface expression levels were significantly increased for ICAM1 (Figure 3D) and a tendency was observed for CD86 (Figure 3E) upon MVA infection. Moreover, these three membrane-bound molecules were barely detected in the soluble protein-enriched fraction (^{armed}iDC-Prots-SEC), validating the SEC efficacy. These results confirm that MVA infection induces a shift in sEVs identity, as initially observed with PBMC-derived EVs by mass spectrometry. We next assessed whether virus-encoded payloads would efficiently be transferred to the surface of EVs and observed that membrane-bound CD40L was exclusively detected on sEVs from DC2.4 cells infected with the ^{armed}MVA (Figure 3F). We subsequently demonstrated the presentation of the SIINFEKL peptide by mouse MHC class I (H-2K^b) on the surface of sEVs derived from DC2.4 infected with the ^{armed}MVA (Figure 3G), using an antibody that detects only the SIINFEKL epitope when presented by mouse MHC class I. This is likely to support both direct and indirect antigen presentation to T cells, as well as cross-presentation to DC (Buzas 2023). Finally, we quantified the murine IL-12 and found it in different proportion after infection with the ^{armed}MVA. As expected, with approximately 100 times more IL-12, most of this soluble cytokine was recovered in the protein-enriched fraction (^{armed}iDC-Prots-SEC), with a small amount still present in the sEVs fraction (^{armed}iDC-EVs-SEC) following SEC isolation. Although some co-isolation can be observed with UC-isolated sEVs (^{armed}iDC-EVs-UC), the majority was likely discarded in the supernatant during UC-based isolation (Figure 3H). Taken together, our findings demonstrate that infection of DC with an armed MVA profoundly alters the molecular composition of their secreted EVs, resulting in (i) modified cargo content, (ii) enrichment of their surface with immunomodulatory cellular molecules such as ICAM-1, and (iii) incorporation of virus-encoded payloads including CD40L, MHC-I/SIINFEKL complexes, and small amount of IL-12. In conclusion, we demonstrated that the infection of mouse DC with an ^{armed}MVA generates EVs with immunomodulatory potential likely to shape an anti-tumoral immune response.

20013078, 2026, 6, Downloaded from https://isevjournals.onlinelibrary.wiley.com/doi/10.1002/jev2.70307 by Cochrane France, Wiley Online Library on [19/06/2026]. See the Terms and Conditions (https://onlinelibrary.wiley.com/terms-and-conditions) on Wiley Online Library for rules of use; OA articles are governed by the applicable Creative Commons License

TABLE 2 | Mass spectrometry on EVs isolated by ultracentrifugation following 200 nm filtration.

ID	protein_set_id	Origin	logFC	P_Value
ORF65|O57179	48279	Viral (MVA)	6,785500254	2,53504E-06
ORF182|6BED_A	50908	Viral (MVA)	6,30328051	2,32152E-07
ORF171|O57211	47286	Viral (MVA)	5,838746512	2,72638E-06
ORF201|AAT10519	47600	Viral (MVA)	5,633137556	3,5616E-07
ORF98|O93117	49813	Viral (MVA)	5,569670255	3,07741E-07
ORF145|AAB96447	48599	Viral (MVA)	5,542520539	6,68678E-07
sp|B1AK53|ESPN_HUMAN	46927	Cellular	5,422910556	4,88433E-07
ORF241|AAB96529	47790	Viral (MVA)	4,967877506	1,1978E-06
ORF288|O57254	47647	Viral (MVA)	4,863000169	2,21972E-06
ORF188|AAB96457	47770	Viral (MVA)	4,398005028	0,000150088
ORF194|AAB96459	48263	Viral (MVA)	4,344466586	3,61714E-05
ORF240|AAB96528	47718	Viral (MVA)	4,147318179	5,85702E-05
ORF101|AAB96435	48160	Viral (MVA)	4,053566656	0,000511299
sp|Q9UBC5|MYO1A_HUMAN	50314	Cellular	3,831759678	0,000157693
sp|Q5ZJ06|MAGT1_CHICK	49900	Cellular	3,772913117	0,001087072
sp|Q9Y3Z3|SAMH1_HUMAN	48298	Cellular	3,709136492	0,000579258
sp|P63243|RACK1_BOVIN	49348	Cellular	3,645079628	0,000474251
ORF260|O57245	47345	Viral (MVA)	3,522518595	0,000168627
sp|P07437|TBB5_HUMAN	50856	Cellular	3,281091297	0,002510495
sp|P02771|FETA_HUMAN	48748	Cellular	3,223497519	5,5736E-06
CON_sp|P42212|GFP_AEQVI	48779	Viral (MVA)	3,155163401	2,52175E-05
sp|P41218|MNDA_HUMAN	48032	Cellular	3,084026384	0,000228116
sp|P14618|KPYM_HUMAN	51339	Cellular	3,028462513	0,001414749
sp|P22451|RL5_CHICK	48453	Cellular	2,998402106	0,000119056
sp|B5ME19|EIFCL_HUMAN	48231	Cellular	2,829889805	0,000305748
sp|O13268|PSA7_CHICK	51334	Cellular	2,756909542	1,63274E-05
sp|P42558|RAN_CHICK	48962	Cellular	2,689956445	0,00049373
sp|P07737|PROF1_HUMAN	49840	Cellular	2,440438947	5,24603E-05
ORF124|O57198	47343	Viral (MVA)	2,38172452	0,002272499
sp|P05109|S10A8_HUMAN	48486	Cellular	2,227652427	0,001137909
ORF77|AAB96428	47022	Viral (MVA)	2,081020348	0,000715572
sp|P35998|PRS7_HUMAN	49136	Cellular	2,078003764	0,001554344
sp|O14672|ADA10_HUMAN	49134	Cellular	2,066206849	0,001004145
ORF74|AAB96427	47459	Viral (MVA)	1,867794252	0,000402186
sp|Q7Z6K1|THAP5_HUMAN	48345	Cellular	1,858398497	7,01518E-05
ORF149|YP_232985	49495	Viral (MVA)	1,681352103	0,00287639
sp|P61157|ARP3_BOVIN	49252	Cellular	1,639792801	0,005437253
sp|P62913|RL11_HUMAN	48619	Cellular	0,818889721	0,002274088
sp|O15371|EIF3D_HUMAN	48101	Cellular	0,81263124	0,003303318
sp|P05556|ITB1_HUMAN	48751	Cellular	−0,903362342	6,88335E-05
sp|P01009|A1AT_HUMAN	47337	Cellular	−1,745351159	0,000707478

Note: Proteins differentially expressed between mock and MVA infected PBMCs are shown (p-value < 0,01). Positive log fold change (logFc): increased expression post-infection. Negative log fold change (logFc): decreased expression post-infection. Chick peptides might originate from initial viral production in chicken embryo fibroblast. Data presented on Figure 2 and Supplementary Figure 3.

20013078, 2026, 6, Downloaded from https://isevjournals.onlinelibrary.wiley.com/doi/10.1002/jev2.70307 by Cochrane France, Wiley Online Library on [19/06/2026]. See the Terms and Conditions (https://onlinelibrary.wiley.com/terms-and-conditions) on Wiley Online Library for rules of use; OA articles are governed by the applicable Creative Commons License

TABLE 3 | Mass spectrometry on EVs isolated by ultracentrifugation following 100 nm filtration.

ID	protein_set_id	Origin	logFC	P_Value
ORF65|O57179	48279	Viral (MVA)	6,885692488	1,82931E-08
ORF171|O57211	47286	Viral (MVA)	6,443348797	7,03973E-10
ORF182|6BED_A	50908	Viral (MVA)	6,435763021	4,72261E-09
ORF145|AAB96447	48599	Viral (MVA)	5,984687536	1,08561E-08
ORF98|O93117	49813	Viral (MVA)	5,634972438	2,36895E-10
ORF201|AAT10519	47600	Viral (MVA)	5,485034833	1,46595E-08
sp|B1AK53|ESPN_HUMAN	46927	Cellular	5,358052449	4,21779E-11
ORF241|AAB96529	47790	Viral (MVA)	5,35400516	2,67466E-07
ORF288|O57254	47647	Viral (MVA)	5,219391302	5,55179E-09
CON_sp|P04264|K2C1_HUMAN	51291	Cellular	5,145592527	0,00067131
CON_sp|P35527|K1C9_HUMAN	51154	Cellular	4,685493508	0,00220051
ORF188|AAB96457	47770	Viral (MVA)	4,51723879	1,9178E-08
ORF194|AAB96459	48263	Viral (MVA)	4,481700474	7,0699E-07
ORF240|AAB96528	47718	Viral (MVA)	4,387995553	1,02921E-07
sp|Q9Y3Z3|SAMH1_HUMAN	48298	Cellular	4,290915337	8,93628E-05
CON_sp|P13645|K1C10_HUMAN	51152	Cellular	4,249755597	0,000509677
sp|P63243|RACK1_BOVIN	49348	Cellular	4,215392512	5,93744E-06
sp|Q5ZJ06|MAGT1_CHICK	49900	Cellular	4,214739212	3,29809E-06
ORF101|AAB96435	48160	Viral (MVA)	4,148582235	1,84462E-06
CON_sp|P35908|K22E_HUMAN	51305	Cellular	3,930851291	0,006558339
sp|P07437|TBB5_HUMAN	50856	Cellular	3,771130487	0,002615998
sp|Q96Q89|KI20B_HUMAN	48380	Cellular	3,545867354	0,001383969
ORF124|O57198	47343	Viral (MVA)	3,384079974	1,01294E-08
sp|P22451|RL5_CHICK	48453	Cellular	3,273708542	3,73446E-05
sp|P08514|ITA2B_HUMAN	49199	Cellular	3,149540912	0,00419256
sp|B5ME19|EIFCL_HUMAN	48231	Cellular	3,083308044	2,89882E-05
CON_sp|P42212|GFP_AEQVI	48779	Viral (MVA)	3,073072887	0,000145159
sp|P02771|FETA_HUMAN	48748	Cellular	2,989160646	0,000253087
sp|P05164|PERM_HUMAN	47605	Cellular	2,968404018	0,000294546
ORF130|YP_717401	47638	Viral (MVA)	2,8643075	2,6349E-06
sp|P35998|PRS7_HUMAN	49136	Cellular	2,859086331	0,005354118
sp|P42558|RAN_CHICK	48962	Cellular	2,813743541	0,002256829
sp|P08133|ANXA6_HUMAN	50465	Cellular	2,692223357	0,005900159
sp|P05107|ITB2_HUMAN	49866	Cellular	2,599461584	0,008379042
ORF30|Q85339	50137	Viral (MVA)	2,560973608	0,000129389
ORF77|AAB96428	47022	Viral (MVA)	2,559046429	0,000629373
sp|P13796|PLSL_HUMAN	49788	Cellular	2,554478111	0,007378767
ORF262|AAB96538	49225	Viral (MVA)	2,539705348	8,30042E-05
ORF260|O57245	47345	Viral (MVA)	2,507873361	0,00069247
sp|P62194|PRS8_BOVIN	49853	Cellular	2,483938825	4,47629E-05
sp|P30740|ILEU_HUMAN	50503	Cellular	2,464304976	0,004269169
sp|P61978|HNRPK_HUMAN	50446	Cellular	2,451879431	0,000276726
sp|A7MB62|ARP2_BOVIN	48268	Cellular	2,38480773	0,005921656

(Continues)

20013078, 2026, 6, Downloaded from https://isevjournals.onlinelibrary.wiley.com/doi/10.1002/jev2.70307 by Cochrane France, Wiley Online Library on [19/06/2026]. See the Terms and Conditions (https://onlinelibrary.wiley.com/terms-and-conditions) on Wiley Online Library for rules of use; OA articles are governed by the applicable Creative Commons License

TABLE 3 | (Continued)

ID	protein_set_id	Origin	logFC	P_Value
sp|O13268|PSA7_CHICK	51334	Cellular	2,340166118	0,000132737
sp|P62269|RS18_HUMAN	49458	Cellular	2,165804048	0,000473002
sp|P55290|CAD13_HUMAN	47742	Cellular	2,125830331	0,002068923
sp|P04899|GNAI2_HUMAN	50441	Cellular	2,003501854	0,002988385
sp|P11940|PABP1_HUMAN	49491	Cellular	1,990701226	0,000107918
sp|P29350|PTN6_HUMAN	50196	Cellular	1,985912444	0,002538262
sp|P26641|EF1G_HUMAN	50234	Cellular	1,968678577	0,008038938
sp|P62244|RS15A_HUMAN	49425	Cellular	1,966086958	0,007798067
sp|Q2HJG5|VPS35_BOVIN	50715	Cellular	1,89017435	0,00106423
ORF149|YP_232985	49495	Viral (MVA)	1,885764905	0,0006268
sp|P51149|RAB7A_HUMAN	49250	Cellular	1,858026268	0,001803068
sp|P07737|PROF1_HUMAN	49840	Cellular	1,821582228	0,00307117
sp|P38919|IF4A3_HUMAN	48909	Cellular	1,771131056	0,003290697
sp|P62249|RS16_HUMAN	50729	Cellular	1,652326029	0,007393382
sp|A6NI72|NCF1B_HUMAN	50975	Cellular	1,627696436	0,006089136
sp|P49721|PSB2_HUMAN	48797	Cellular	1,614769426	0,007315169
sp|P43686|PRS6B_HUMAN	49852	Cellular	1,597906995	0,004932369
sp|P62998|RAC1_BOVIN	49202	Cellular	1,539752321	0,002989771
sp|P62333|PRS10_HUMAN	50302	Cellular	1,511164791	0,006854742
sp|P07195|LDHB_HUMAN	49715	Cellular	1,451829455	0,004330675
sp|P00558|PGK1_HUMAN	51183	Cellular	1,448782144	0,00525885
sp|P26038|MOES_HUMAN	50073	Cellular	1,384645213	0,004447246
sp|Q96CX2|KCD12_HUMAN	49089	Cellular	1,348359167	0,00033986
sp|P48463|PP2AA_CHICK	49708	Cellular	1,265541156	0,002457297
sp|P60706|ACTB_CHICK	50877	Cellular	1,248988163	0,006211273
sp|O15371|EIF3D_HUMAN	48101	Cellular	1,198370659	0,001809224
sp|P59998|ARPC4_HUMAN	47836	Cellular	1,077804707	7,93772E-05
sp|P00517|KAPCA_BOVIN	50692	Cellular	0,81333298	0,000123056
sp|A6QLG5|RS9_BOVIN	47225	Cellular	0,811676446	2,63585E-05
sp|Q0P5A6|PSMD5_BOVIN	48433	Cellular	0,714868769	0,009285614
sp|P01009|A1AT_HUMAN	47337	Cellular	−1,124685107	0,005888906
sp|P62801|H4_CHICK	50326	Cellular	−1,708300395	2,87504E-06

Note: Proteins differentially expressed between mock and MVA infected PBMCs are shown (p-value < 0,01). Positive log fold change (logFc): increased expression post-infection. Negative log fold change (logFc): decreased expression post-infection. Chick peptides might originate from initial viral production in chicken embryo fibroblast. Data presented on Figure 2 and Supplementary Figure 3>.

10.4 | sEVs Secreted by DC Infected With an Armed MVA Activate and Expand CD8$^+$ T Cells

To assess this immunomodulatory potential, we next investigated whether sEVs secreted by ^{armed}MVA-infected DC could directly stimulate SIINFEKL-specific CD8$^+$ T cells *in vitro*. To this end, we isolated naïve CD8$^+$ T cells from the spleens of OT-I transgenic mice, which express a TCR specific for the OVA-derived peptide SIINFEKL presented by the murine MHC class I molecule H-2K^b. These naïve CD8$^+$ T cells were stimulated for 3 days with sEVs or the protein-enriched fraction secreted by ^{armed}MVA-infected DC. We measured CD8$^+$ T cell activation and proliferation by flow cytometry (Figure 4A) and observed that ^{armed}iDC-EVs UC induced a strong CD8$^+$ T cell activation, as probed by CD44 expression, to levels comparable to the positive control stimulated with anti-CD3/CD28 antibodies (Figure 4B). By contrast, sEVs from non-infected DC (DC-EVs UC) or from cells infected with an empty MVA (^{empty}iDC-EVs-UC) failed to induce the activation of CD8$^+$ T cells (Figure 4B), while ^{armed}iDC-EVs-SEC induced a moderate CD8$^+$ T cells activation and the protein-enriched

20013078, 2026, 6, Downloaded from https://isevjournals.onlinelibrary.wiley.com/doi/10.1002/jev2.70307 by Cochrane France, Wiley Online Library on [19/06/2026]. See the Terms and Conditions (https://onlinelibrary.wiley.com/terms-and-conditions) on Wiley Online Library for rules of use; OA articles are governed by the applicable Creative Commons License

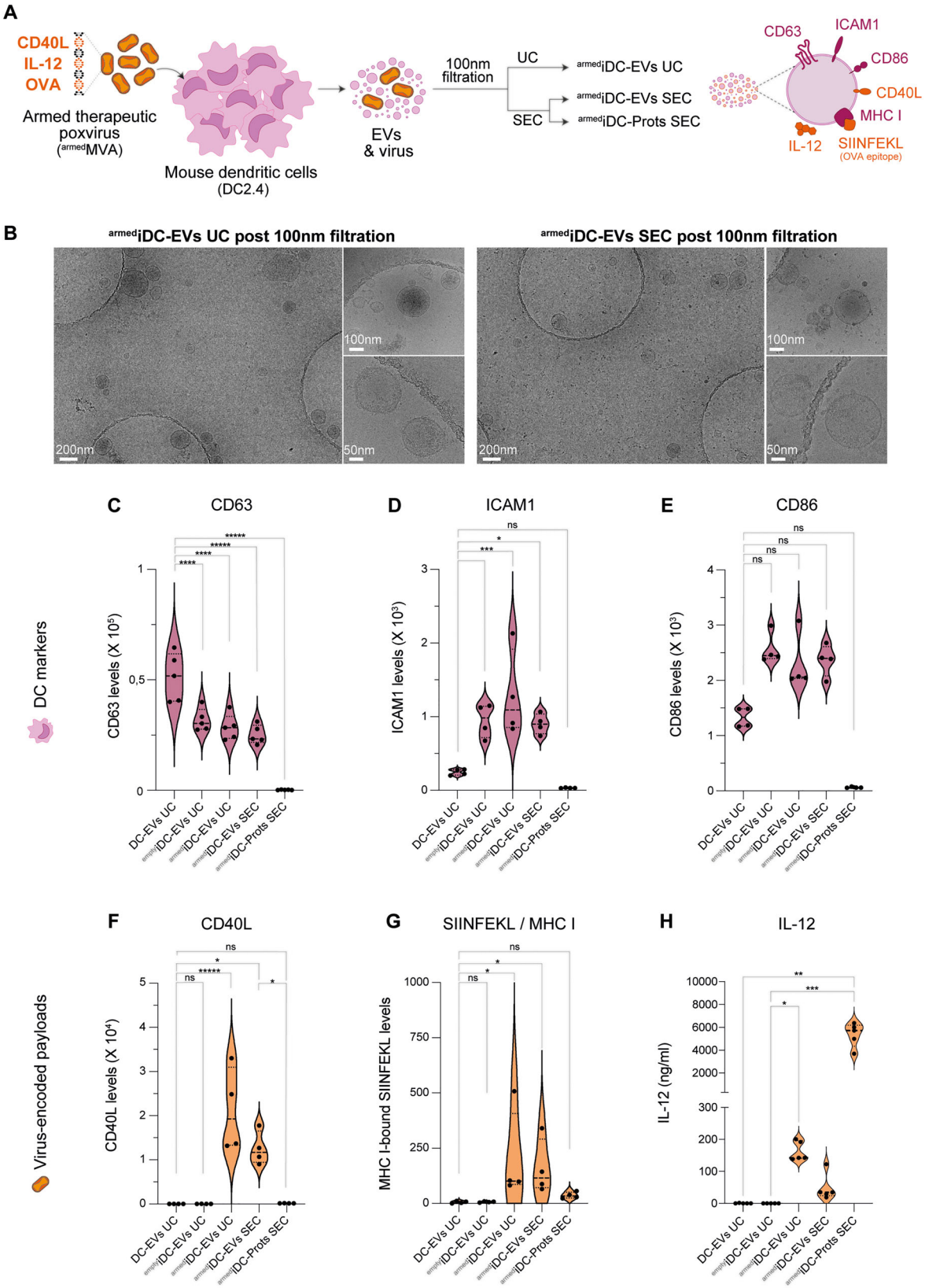


FIGURE 3 | : Virus-encoded therapeutic payloads are retrieved in small EVs. A) Workflow for assessing the presence of cellular proteins (CD63, ICAM1 and CD86) and virus-encoded therapeutic payloads (IL-12, CD40L and OVA peptide SIINFEKL presented on MHCI) on EVs secreted by mouse dendritic cells (DC2.4) and isolated by ultracentrifugation (UC) or size exclusion chromatography (SEC; EVs-rich fractions (EVs SEC, fractions 1–4) and soluble proteins-rich fractions (Prots SEC, fractions 5–10)) following 100 nm filtration. B) Cryo-EM images of EVs isolated by UC (left) or SEC (right) post-100 nm filtration from DC2.4 cells infected with the armed MVA virus. (C–H) Payloads were quantified by electrochemiluminescence immunoassay on

20013078, 2026, 6, Downloaded from https://isevjournals.onlinelibrary.wiley.com/doi/10.1002/jev2.70307 by Cochrane France, Wiley Online Library on [19/06/2026]. See the Terms and Conditions (https://onlinelibrary.wiley.com/terms-and-conditions) on Wiley Online Library for rules of use; OA articles are governed by the applicable Creative Commons License

fractions ([armed]iDC-Prots-SEC), almost none. Further analysis of T cells proliferation revealed that [armed]iDC-EVs-UC induced CD8$^+$ T cells proliferation up to six cell generations (G0 to G6), with approximately twice as many cells in generations G5–G6, rising from 9,77% in the positive control to 18,18%. Consistent with their lack of activation, CD8$^+$ T cells stimulated with either DC-EVs-UC or [empty]iDC-EVs-UC mostly remained in generation G0, similar to the unstimulated control. On the other hand, [armed]iDC-EVs-SEC and [armed]iDC-Prots-SEC had weaker effects and show highly heterogeneous CD8$^+$ T cell proliferation patterns (Figure 4C and Figure S5A). We further demonstrate that efficient CD8$^+$ T cell activation relies on antigen presentation by sEVs, since MHC I/SIINFEKL blocking antibody (previously described by Blair et al. 2011) reduced CD8$^+$ T cell proliferation in a dose-dependent manner (Figure S5B). Altogether, our results demonstrate that sEVs isolated from DC2.4 infected with an armed MVA are able to activate specific CD8$^+$ T cells and induce their proliferation in vitro, suggesting that they could also trigger a potent T-cell mediated antitumoral response in vivo.

10.5 | sEVs Released by DC Infected with an Armed MVA Prevent Tumor Growth

To assess the therapeutic potential of these sEVs secreted by [armed]MVA-infected DC, we injected intravenously mice bearing E.G7-OVA lymphoma with sEVs or the protein-enriched fraction at days D7 and D14 post-tumor inoculation (Figure 5A). PBS and the [armed]MVA virus were used as controls. We observed that both, UC- and SEC-isolated sEVs from [armed]MVA-infected DC, significantly reduced tumor growth, to levels obtained when mice were injected with the [armed]MVA virus itself (Figure 5B–C). By contrast, in mice injected with EVs isolated from cells infected with an empty MVA virus, tumors grew to a similar extent than in PBS-treated mice (Figure S5C). Notably, tumor growth patterns were very similar when mice were treated with [armed]iDC-EVs-UC or the [armed]MVA (Figure 5B). Accordingly, survival of mice at D21 was significantly improved when treated with [armed]iDC-EVs UC, compared to other treatments (Figure 5B). While similar antitumoral efficacy was obtained with the protein-enriched fraction ([armed]iDC-Prots-SEC) obtained from [armed]MVA-infected DC, sEVs from non-infected DC (DC-EVs-UC) had no effect on tumor growth. Measures at D21 revealed that sEVs or protein-enriched fraction from [armed]MVA-infected DC could reduce tumor growth to levels obtained with the [armed]MVA only (Figure 5C). To understand the underlying mechanism, we isolated and quantified at D21 the number of OVA-specific T cells in the peripheral blood of mice bearing an E.G7-OVA mouse lymphoma. While we detected SIINFEKL-specific CD8$^+$ T cells in all groups treated with sEVs or protein-enriched fraction isolated from [armed]MVA-infected DC (Figure S5D), these were 10 to 50 times less abundant than in the [armed]MVA virus-treated group. Altogether, our data demonstrate that the secretome (EV-bound and soluble) of DC infected by a fully armed MVA is as effective as the armed MVA alone in impairing the progression of the E.G7-OVA mouse lymphoma model, likely via controlling immunosurveillance.

11 | Discussion

Therapeutic vaccination is increasingly recognized as a new modality of immunotherapy, with accumulating preclinical and clinical evidence supporting its efficacy in inducing robust antitumor immune responses (Pail et al. 2025). Yet, the underlying molecular and cellular mechanisms remain incompletely characterised. In this study, we demonstrate that poxvirus-based vaccination induces the secretion of anti-tumoral sEVs by infected immune cells. Our in vitro and in vivo analyses indicate that these sEVs may constitute a key component of the vaccine-induced antitumor response, acting as mediators of antigen presentation and immune modulators, and may themselves hold promising potential as standalone therapeutic agents. To explore this potential, further work will be required to expand our initial observations to other viral strains than MVA and to other infected cell types. In addition, the function of larger EVs, which could not be collected using our filtration-based isolation method, will have to be investigated.

The similarities between EVs and viruses represents a significant challenge in the development of a universal separation method, due to their overlapping physical and biochemical properties, including size, density, membrane composition, and biogenesis pathways as well as the structural diversity among viral species (Nolte-'t Hoen et al. 2016; Minh and Kamen, 2021). For these reasons, some of the methods approved with other viruses, such as density gradient for hCMV (Bergamelli et al. 2021) or velocity gradient for HIV (Martin-Jaular et al., 2021) have not proven effective for poxvirus in our study. By contrast, combining

EVs isolated from non-infected cells (mock) or from cells infected with empty or armed MVA virus (encoding IL12, CD40L and OVA peptide SIINFEKL payloads). C) Quantification of CD63 on EVs. EVs mock Vs EVs empty virus $p = 0{,}0007$; EVs mock Vs EVs armed virus UC $p = 0{,}0001$; EVs mock Vs EVs armed virus SEC $p < 0{,}0001$; EVs mock Vs Soluble proteins armed virus SEC $p < 0{,}0001$; One-way Anova; $N = 5$ independent experiments. D) Quantification of ICAM1 on EVs. EVs mock Vs EVs empty virus: $p = 0{,}0276$; EVs mock Vs EVs armed virus UC $p = 0{,}0012$; EVs mock Vs EVs armed virus SEC $p = 0{,}0425$; EVs mock Vs Soluble proteins armed virus SEC $p = 0{,}83$; One-way Anova; $N = 4$ independent experiments. E) Quantification of CD86 on EVs. EVs mock Vs EVs empty virus: $p = 0{,}19$; EVs mock Vs EVs armed virus UC $p > 0{,}99$; EVs mock Vs EVs armed virus SEC $p = 0{,}73$; EVs mock Vs Soluble proteins armed virus SEC $p = 0{,}99$; Kruskal-Wallis; $N = 4$ independent experiments. F) Quantification of CD40L on EVs. EVs mock Vs EVs empty virus: $p > 0{,}99$; EVs mock Vs EVs armed virus UC $p < 0{,}0001$; EVs mock Vs EVs armed virus SEC $p = 0{,}011$; EVs mock Vs Soluble proteins armed virus SEC $p > 0{,}99$; EVs armed virus SEC Vs Soluble proteins armed virus SEC $p = 0{,}0125$; One-way Anova; $N = 4$ independent experiments. G) Quantification of MHCI bound OVA peptide (SIINFEKL). EVs mock Vs EVs empty virus: $p > 0{,}99$; EVs mock Vs EVs armed virus UC $p = 0{,}023$; EVs mock Vs EVs armed virus SEC $p = 0{,}0341$; EVs mock Vs Soluble proteins armed virus SEC $p > 0{,}99$; Kruskal-Wallis; $N = 4$ independent experiments. H) Quantification of IL-12. EVs mock Vs Soluble proteins armed virus SEC $p = 0{,}0051$; EVs empty virus Vs EVs armed virus UC $p = 0{,}0236$; EVs empty virus Vs Soluble proteins armed virus SEC $p = 0{,}0004$; Kruskal-Wallis test. $N = 5$ independent experiments. * $p < 0{,}05$; ** $p < 0{,}01$; *** $p < 0{,}005$; **** $p < 0{,}001$; ***** $p < 0{,}0001$; ns: non-significant.

20013078, 2026, 6, Downloaded from https://isevjournals.onlinelibrary.wiley.com/doi/10.1002/jev2.70307 by Cochrane France, Wiley Online Library on [19/06/2026]. See the Terms and Conditions (https://onlinelibrary.wiley.com/terms-and-conditions) on Wiley Online Library for rules of use; OA articles are governed by the applicable Creative Commons License

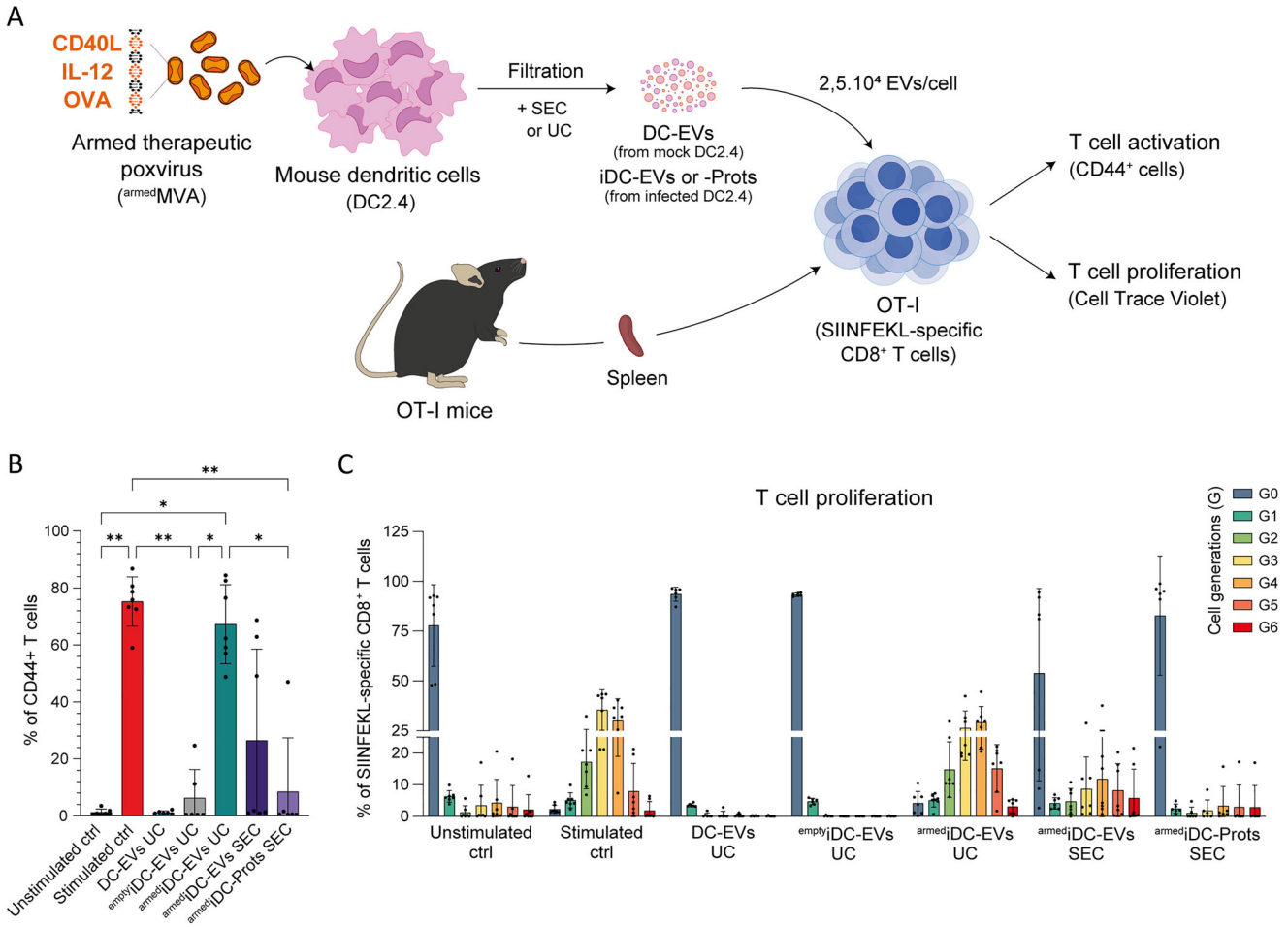


FIGURE 4 | : EVs isolated from therapeutic virus-infected dendritic cells activate and stimulate anti-tumoral cytotoxic T cells in vitro. (A) Workflow for testing the ability of EVs to activate OVA-specific CD8+ T cells in vitro and stimulate their proliferation. EVs were isolated by ultracentrifugation (UC) or size exclusion chromatography (SEC) following 100 nm filtration, from non-infected murine dendritic cells (DC-EVs UC), or infected with an empty MVA virus (emptyiDC-EVs UC), or with an armed MVA virus (encoding IL-12, CD40L and OVA peptide SIINFEKL payloads) yielding armediDC-EVs UC for EVs isolated by UC, armediDC-EVs SEC for EVs isolated by SEC and armediDC-Prots SEC for the soluble fraction isolated by SEC. PBS was used as a negative control (Unstimulated ctrl) and anti-CD3/CD28 antibodies as a positive control to activate T cells (Stimulated ctrl). (B) Levels of T cells activation marker CD44 quantified by cytometry. Unstimulated ctrl Vs Stimulated ctrl $p = 0{,}0056$; Stimulated ctrl Vs iDC-EVs UC (empty virus) $p = 0{,}0033$; Unstimulated ctrl Vs iDC-EVs UC (armed virus) $p = 0{,}0245$; Stimulated ctrl Vs iDC-Prots SEC (armed virus) $p = 0{,}0075$; iDC-EVs UC (empty virus) Vs iDC-EVs UC (armed virus) $p = 0{,}0143$; iDC-EVs UC (armed virus) Vs iDC-Prots SEC (armed virus) $p = 0{,}0303$; Kruskal-Wallis. No significant difference in the absence of stars. $n = 1$ to 2 replicates per group, in $N = 4$ independent experiments. * $p < 0{,}05$; ** $p < 0{,}01$. C) Quantification of the number of T cells per generation (from G0 to G6) following stimulation with positive control or with EVs. $n = 1$ to 2 replicates per group, in $N = 4$ independent experiments.

100 nm filtration with UC or SEC effectively isolates sEVs from infectious MVA or VV_{COP} particles. While this approach allowed us to unambiguously demonstrate that sEVs released post-infection contain virus-encoded payloads and bear anti-tumoral immunomodulatory functions, it is also possible that bigger EVs possess similar properties. Although our study is limited to poxviral strains, our isolation method could be easily applied to the study of sEVs secreted by cells infected with other viruses exceeding 100 nm in size, such as the Epstein–Barr virus (Henson et al. 2009), the Sendai virus (Fujita et al. 2006) or the Varicella-zoster virus (Sun et al. 2020).

Our work demonstrates that poxvirus infection triggers a five-fold increase in sEVs secretion by immune cells. Similarly, oncolytic poxviruses (including the vaccinia virus) targeting tumor cells were recently shown to increase the secretion of EVs and modify their content (Hirigoyen et al. 2024). These findings align with previous reports involving other viral families, such as Enterovirus 71 (Fu et al. 2017), rotavirus RRV (Iša et al. 2020), hepatitis A virus (Jiang et al. 2020), astrovirus (Baez-Navarro et al. 2022), and picornavirus (Defourny et al. 2024) and supports the notion that increased EVs secretion is a common cellular response to viral infection. Whether this response relates to the increased EV secretion observed after cellular stress (induced by heat, hypoxia or H2O2) (Singh et al. 2025) remains to be determined. While each virus may exploit distinct host pathways, including hijacking the endosomal and MVB pathways, activation of stress and inflammatory responses, and extensive remodelling of the cytoskeleton and membrane trafficking machinery; the convergence on EV-associated path-

20013078, 2026, 6, Downloaded from https://isevjournals.onlinelibrary.wiley.com/doi/10.1002/jev2.70307 by Cochrane France, Wiley Online Library on [19/06/2026]. See the Terms and Conditions (https://onlinelibrary.wiley.com/terms-and-conditions) on Wiley Online Library for rules of use; OA articles are governed by the applicable Creative Commons License

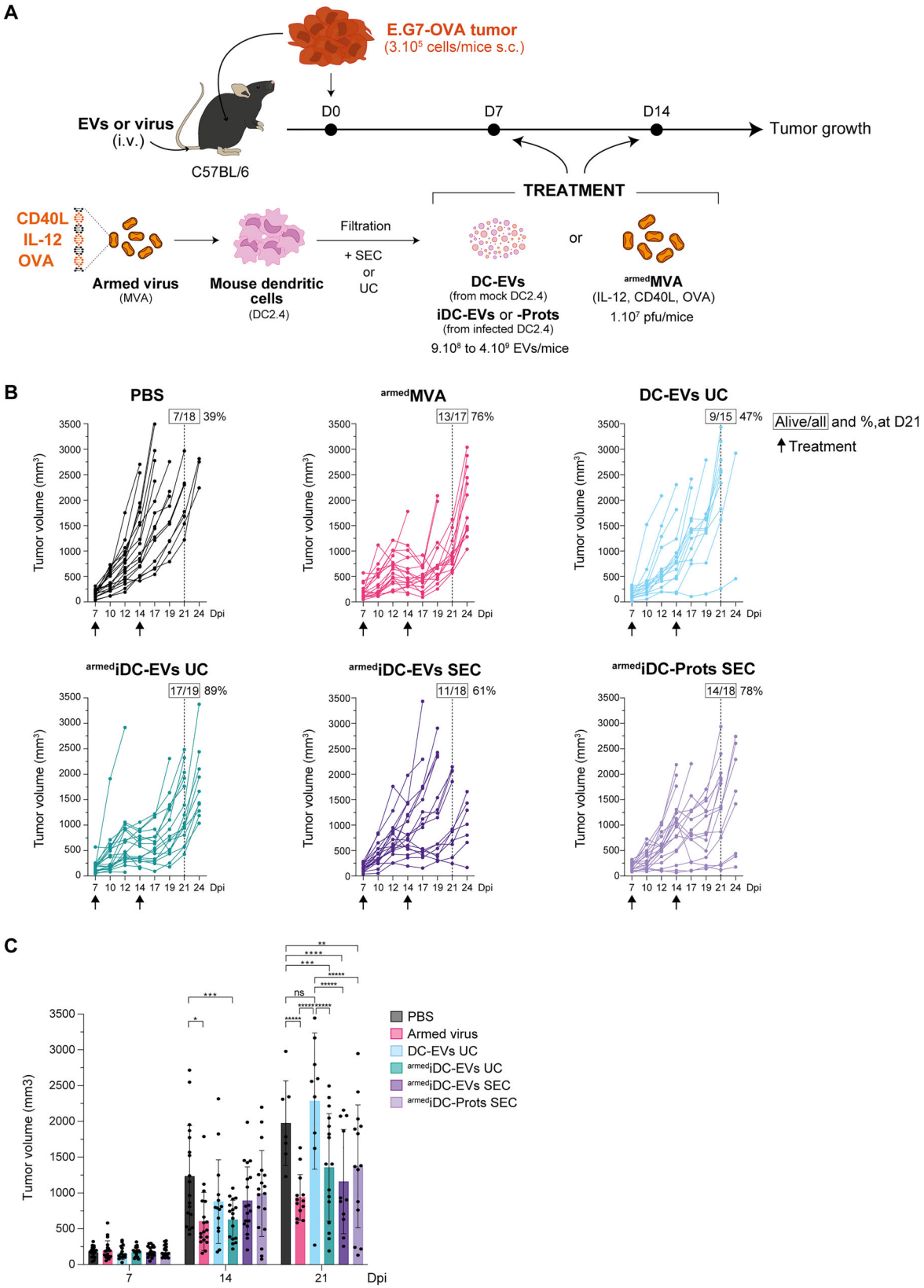


FIGURE 5 | : EVs isolated from therapeutic virus-infected dendritic cells inhibit tumor progression in vivo. A) Workflow for assessing the anti-tumoral potential of EVs secreted by mouse dendritic cells (DC2.4) isolated by ultracentrifugation (UC) or size exclusion chromatography (SEC; EVs-rich fractions (EVs SEC, fractions 1–4) and soluble proteins-rich fractions (Prots SEC, fractions 5–10)) following 100 nm filtration. EVs were isolated from non-infected cells (mock) or from cells infected with empty or armed MVA virus (encoding IL-12, CD40L and OVA peptide SIINFEKL payloads). EVs were injected intravenously 7- and 14-days post E.G7-OVA tumor cell injection and tumor growth was monitored for 24 days. B) Tumor growth curves of

20013078, 2026, 6, Downloaded from https://isevjournals.onlinelibrary.wiley.com/doi/10.1002/jev2.70307 by Cochrane France, Wiley Online Library on [19/06/2026]. See the Terms and Conditions (https://onlinelibrary.wiley.com/terms-and-conditions) on Wiley Online Library for rules of use; OA articles are governed by the applicable Creative Commons License

ways, demonstrates a shared strategy of leveraging host cell biology. This evolutionary convergence likely results in altered EV-mediated cell communication from infected cells, which could in turn impact antiviral immunity. While the mechanisms by which poxviruses promote EV secretion are unknown and were not studied here, EV content analysis might provide some hints. We found that sEVs secreted post-infection display reduced surface levels of CD63, a tetraspanin mostly present on MVB where is sorts cholesterol to nascent exosomes (Palmulli et al. 2024). Decrease in CD63 levels, could be related to the capacity of poxvirus to hijack the cellular ESCRT machinery and induce viral maturation in MVBs, as shown for the vaccinia virus (Huttunen et al. 2021). We hypothesize that the exploitation of the host machinery responsible for exosome biogenesis by poxvirus diverts the function of the ESCRT complex, thereby decreasing the generation of CD63-positive exosomes. In addition, we observed that EVs secreted post-infection are enriched in actin regulators, including host MYO1A (McConnell et Tyska 2007), ESPIN (Bartles et al. 1996; Rajan et al. 2023), profilin and the Arp2/3 complex member ARPC4 (Bieling et Rottner 2023). This signature might relate to the ability of poxviruses to rapidly remodel actin in order to propel themselves within the cytoplasm (Frischknecht et al. 1999; Dodding and Way 2009; Doceul et al. 2010). Since actin remodelling has been associated to EV secretion, both from the plasma membrane (Muralidharan-Chari et al. 2009) and from MVBs (Sinha et al. 2016), we speculate that poxvirus promote EV secretion by manipulating the actin cytoskeleton. While the precise mechanisms through which poxvirus modulate EV secretion remain to be deciphered, they are likely to involve viral proteins. Among possible candidates, three viral proteins are present in sEVs post-infection and could be involved in boosting EV secretion: B5 and A34, which are known to manipulate host actin cytoskeleton (Wolffe et al. 1997; Doceul et al. 2010), and F13, which associates to late endosomes (Grosenbach et al. 1997; Honeychurch et al. 2007). Mapping precisely which EV biogenesis pathways are disrupted, and which subpopulations of EVs are affected by poxvirus infection, will deepen our understanding of virus–host interactions to notably assist in the detection and control of future outbreaks (e.g., mpox, caused by monkeypox virus), using EVs as biomarkers, targets or vaccine vectors. It also reveals opportunities to enhance EV secretion for therapeutic applications, as controlled infection of production cells combined with optimized isolation workflows, could be harnessed to enhance EV yields and support scalable biomanufacturing, thus providing an additional innovative strategy to the methods currently explored (Ng et al. 2022).

Manipulation of EV biogenesis by poxviruses might also directly affect their capacity to modulate the immune response. We found that MVA infection of immune cells promotes the accumulation of known mediators of inflammation, either coming from the host cell, such as SAMHD1 (Chen et al. 2019), Rack1 (Usacheva et al. 2001; Yao et al. 2014) or ICAM1 (Bui et al. 2020) or from the virus, including B8 (Symons and Smith 1995) and A46 (Stack and Bowie 2012). Besides, those EVs also contain viral proteins known to be involved in virus uptake or fusion, such as H3, D8 and B5 (Lin et al. 2000; Roberts et al. 2009; Pokorny et al. 2024) and could therefore have altered internalization route and downstream signaling. More relevant for EV engineering and therapeutic purposes, we identified the transfer of virus-encoded payloads to EVs secreted post-infection: membrane-bound CD40L, the OVA epitope SIINFEKL presented by MHC class I as well as a fraction of the soluble cytokine IL-12 that was co-isolated with sEVs. EV transfer of virus-encoded payloads offers additional opportunities to amplify the therapeutic efficacy of the vector, for instance by enhancing the enrichment of the payloads in EVs. While the relative contribution of each EV-associated payload to the anti-tumoral effect remains to be determined, we speculate that the combination of the three payloads provides an enhanced response, based on what we observed when comparing anti-tumor efficacy of single, double and triple armed virus (Figure S4). We expect a complementary effect of IL12 and CD40L, acting respectively on $CD8^+$ T cells differentiation (Mirlekar et Pylayeva-Gupta 2021; Bella et al. 2023), and on DC maturation, NK cells and T cell activation (Elgueta et al. 2009; Medina-Echeverz et al. 2019).

Remarkably, we found that EVs secreted by DC infected with an armed virus and isolated by UC or SEC significantly inhibited tumor growth to levels comparable with an armed virus. This suggest that the efficacy of viral therapies could be partially explained by the release of immunocompetent EVs stimulated by viral infection. Interestingly, the soluble secretome from infected cells similarly decreases tumor growth. While this fraction is deprived of CD40L and contains small amounts of the OVA epitope SIINFEKL presented by MHC class I, it is highly enriched in IL-12 and could contain additional factors, including OVA epitopes, present in protein aggregates/exomeres or in soluble form, able to trigger an anti-tumoral immune response after being processed by APC. Although EVs (UC- and SEC-isolated) and soluble factors similarly reduce tumor growth in vivo, it is probable that this is achieved via different mechanisms. Indeed, while EVs isolated by UC induce a strong and direct MHCI-dependent activation and proliferation of OVA-specific T cells *in vitro*, SEC-isolated EVs and soluble fractions only have a moderate effect. Since we detected few but significant amounts of SIINFEKL-specific $CD8^+$ T cells in the circulation of mice, it is possible that SEC-isolated EVs and soluble fractions activate T-cells indirectly, via APC, a mechanism that could be amplified by

individual mice treated with PBS (black), with triple armed MVA virus (pink), with EVs isolated by ultracentrifugation from non-infected cells (mock, light blue) or from cells infected with armed MVA virus (green) or with EVs isolated by size exclusion chromatography (SEC), EVs rich fraction (iDC-EVs SEC, deep purple) or soluble proteins rich fraction (iDC-Prots SEC). Arrows indicate the injection days. Number and percentage of living mice at day 21 are indicated in boxes. One curve represents one mouse, $n = 15$ to 19 mice per group, in $N = 4$ independent experiments. C) Tumor volume at day 7, 14 and 21 post-tumor cell injection. At day 14, PBS Vs Armed virus $p = 0{,}0017$; PBS Vs iDC-EVs UC (armed virus) $p = 0{,}019$. At day 21, PBS Vs Armed virus $p < 0{,}0001$; PBS Vs iDC-EVs UC (armed virus) $p = 0{,}0041$; PBS Vs iDC-EVs SEC (armed virus) $p = 0{,}0005$; PBS Vs iDC-Prots SEC (armed virus) $p = 0{,}0053$; Armed virus Vs DC-EVs UC (mock) $p < 0{,}0001$; iDC-EVs UC (armed virus) Vs DC-EVs UC (mock) $p < 0{,}0001$; iDC-EVs SEC (armed virus) Vs DC-EVs UC (mock) $p < 0{,}0001$ and iDC-Prots SEC (armed virus) Vs DC-EVs UC (mock) $p < 0{,}0001$. Two-way Anova test. No significant difference with PBS in the absence of stars. * $p < 0{,}05$; ** $p < 0{,}01$; *** $p < 0{,}005$; **** $p < 0{,}001$; ***** $p < 0{,}0001$; ns: non-significant.

20013078, 2026, 6, Downloaded from https://isevjournals.onlinelibrary.wiley.com/doi/10.1002/jev2.70307 by Cochrane France, Wiley Online Library on [19/06/2026]. See the Terms and Conditions (https://onlinelibrary.wiley.com/terms-and-conditions) on Wiley Online Library for rules of use; OA articles are governed by the applicable Creative Commons License

elevated IL-12 levels. Of note, the levels of circulating SIINFEKL-specific CD8$^+$ T cells are low compared to the ones found after viral infection, but our analysis was limited to T cells circulating in the peripheral blood, not reflecting what may be occurring in other compartments such as in the tumor microenvironment where higher amount of tumor-infiltrating lymphocytes could be present (Yin et al. 2016). Alternatively, SEC-isolated EVs and soluble fractions could promote tumor cell eradication through CD8$^+$ T-cell-independent mechanisms, which could include cytotoxic NK cells, known to be activated by IL-12 (Ohs et al. 2016; Rademacher et al. 2021). The difference between the abilities of the UC- and SEC-isolated EVs to activate CD8$^+$ T cells could be explained by the fact that UC co-isolates some co-factors (soluble or aggregated) which are removed by SEC. It is therefore possible that direct T cell activation requires the cumulative effect of both soluble and EV-bound SEC fractions, as shown for instance in the case of the platelet secretome, where both fractions are required to promote angiogenesis and wound closure (Gomes et al. 2022). Overall, our work highlights the necessity to precisely characterise the function of each fraction of the secretome, including EVs subpopulations. A better understanding of this complex signaling could open the doors to improved viral vectors further boosting therapeutic cargo loading (Zheng et al. 2023; Chen et al. 2024). Alternatively, EVs could be used as therapeutic vectors, although multiple challenges, including their comprehensive molecular characterization or the potential requirement for patients-derived EVs, will have to be addressed to fully reach the clinics (Kumar et al. 2024).

Altogether our findings demonstrate the anti-tumoral function of sEVs released by immune cells infected with poxviruses. It strengthens the clinical potential of EVs as therapeutics and particularly as vaccine delivery platforms and underscore the importance of considering the entire secretome, as a functionally integrated system capable of driving potent anti-tumor responses.

Author Contributions

Lucas Walther: conceptualization, investigation, writing – original draft, writing – review and editing. **Vincent Mittelheisser**: investigation. **Marie-Christine Claudepierre**: investigation. **Louis Bochler**: investigation. **Magali Rompais**: investigation. **Jules Deforges**: formal analysis. **Nathalie Silvestre**: investigation. **Annabel Larnicol**: investigation. **Christine Carapito**: supervision. **Eric Quémeneur**: supervision. **Jacky G Goetz**: supervision, conceptualization, funding acquisition, writing – original draft, writing – review and editing. **Karola Rittner**: conceptualization, investigation, supervision, writing – original draft, funding acquisition. **Vincent Hyenne**: supervision, conceptualization, investigation, writing – original draft, writing – review and editing, funding acquisition.

Acknowledgements

We thank members of the Tumor Biomechanics Lab and Transgene for helpful discussions. We thank Kuang-Jing Huang for helping with electron microscopy pictures processing. We warmly thank Xavier Huet from Meso Scale Discovery (MSD) for helping with ECL immunoassays data processing. We thank Carine Reymann and Yasmin Schlesinger for the generation of recombinant MVA. We thank members of the CRBS animal facility for animal care and the members of the "Institut Clinique de la Souris" (Illkirch-Graffenstaden, France) who handle the E.G7-OVA in vivo experiments. We thank Alexandre Durand and Corinne Crucifix from the IGBMC ("Institut de Génétique et de Biologie Moléculaire et Cellulaire", Department of Integrative Structural Biology, Illkirch-Graffenstaden, France) for performing part of the cryo-electron microscopy and image acquisition. We thank Benoît Bragantini from the Biophysics and Structural Biology Core Facility of Service Mutualisé de Plateformes (SMP)—Pôle BMS. (Université de Lorrainehttp://umsibslor.univ-lorraine.fr) for performing part of the cryo-electron microscopy and image acquisition. Research was co-funded by Transgene S.A. and a CIFRE PhD fellowship to LW managed by the Association Nationale de la Recherche et de la Technologie, ANRT (grant n°2021/0562). VM was supported by a fellowship from the French Ministry of Science (MESRI) and a fourth-year thesis fellowship from the Fondation ARC pour la recherche sur le cancer (n° ARCDOC42023010006005). LB was funded by PhD fellowship from Fondation pour la Recherche Médicale (n°ECO202206015567). Proteomics analyses were supported by the French National Research Agency ProFI fundings (Proteomics French Infrastructure; ANR-10-INBS-08; ANR-24-INBS-0015). This work was also supported by grants from La Ligue contre le Cancer and by institutional funds from University of Strasbourg and INSERM.

Conflicts of Interest

Lucas Walther, Marie-Christine Claudepierre, Jules Deforges, Nathalie Silvestre, Eric Quéméneur and Karola Rittner are or were employees of Transgene S.A.

Data Availability Statement

The data that support the findings of this study are openly available in Hyenne at https://www.ebi.ac.uk/pride/.

References

Baez-Navarro, C., I. R Quevedo, S. López, C. F Arias, and P. Iša. 2022. "The Association of Human Astrovirus With Extracellular Vesicles Facilitates Cell Infection and Protects the Virus From Neutralizing Antibodies." *Journal of Virology* 96, no. 14:e0084822.

Bartles, J. R., A. Wierda, and L. Zheng. 1996. "Identification and Characterization of Espin, an Actin-Binding Protein Localized to the F-Actin-Rich Junctional Plaques of Sertoli Cell Ectoplasmic Specializations." *Journal of Cell Science* 109, no. Pt 6: 1229–1239. https://doi.org/10.1242/jcs.109.6.1229.

Bella, Á., L. Arrizabalaga, C. A Di Trani, et al. 2023. "Abstract 2736: Locoregional Modified Vaccinia Ankara (MVA) Encoding a Single-chain IL-12 Achieves Efficacy Antitumor Immune Response in Peritoneal Carcinomatosis." *Cancer Research* 83, no. 7: 2736–2736. https://doi.org/10.1158/1538-7445.AM2023-2736.

Bendjama, K., and E. Quemeneur. 2017. "Modified Vaccinia Virus Ankara-Based Vaccines in the era of Personalized Immunotherapy of Cancer." *Human Vaccines & Immunotherapeutics* 13, no. 9: 1997–2003. https://doi.org/10.1080/21645515.2017.1334746.

Bergamelli, M., H. Martin, M. Bénard, et al. 2021. "Human Cytomegalovirus Infection Changes the Pattern of Surface Markers of Small Extracellular Vesicles Isolated From First Trimester Placental Long-Term Histocultures." *Frontiers in Cell and Developmental Biology* 9: 689122. https://doi.org/10.3389/fcell.2021.689122.

Bezeljak, U. 2022. "Cancer Gene Therapy Goes Viral: Viral Vector Platforms Come of Age." *Radiology and Oncology* 56, no. 1: 1–13. https://doi.org/10.2478/raon-2022-0002.

Bieling, P., and K. Rottner. 2023. "From WRC to Arp2/3: Collective Molecular Mechanisms of Branched Actin Network Assembly." *Current Opinion in Cell Biology* 80: 102156. https://doi.org/10.1016/j.ceb.2023.102156.

Blair, D. A., D. L Turner, T. O Bose, et al. 2011. "Duration of Antigen Availability Influences the Expansion and Memory Differentiation of T

20013078, 2026, 6, Downloaded from https://isevjournals.onlinelibrary.wiley.com/doi/10.1002/jev2.70307 by Cochrane France, Wiley Online Library on [19/06/2026]. See the Terms and Conditions (https://onlinelibrary.wiley.com/terms-and-conditions) on Wiley Online Library for rules of use; OA articles are governed by the applicable Creative Commons License

Cells." *The Journal of Immunology* 187, no. 5: 2310–2321. https://doi.org/10.4049/jimmunol.1100363.

Bouyssié, D., A. M Hesse, E. Mouton-Barbosa, et al. 2020. "Proline: An Efficient and User-Friendly Software Suite for Large-Scale Proteomics." *Bioinformatics* 36, no. 10: 3148–3155. https://doi.org/10.1093/bioinformatics/btaa118.

Bromley, S. K., and M. L. Dustin. 2002. "Stimulation of Naïve T-Cell Adhesion and Immunological Synapse Formation by Chemokine-Dependent and -Independent Mechanisms." *Immunology* 106, no. 3: 289–298.

Bui, T. M., H. L. Wiesolek, and R. Sumagin. 2020. "ICAM-1: A Master Regulator of Cellular Responses in Inflammation, Injury Resolution, and Tumorigenesis." *Journal of Leukocyte Biology* 108, no. 3: 787–799. https://doi.org/10.1002/JLB.2MR0220-549R.

Buzas, E. I. 2023. "The Roles of Extracellular Vesicles in the Immune System." *Nature Reviews Immunology* 23, no. 4: 236–250. https://doi.org/10.1038/s41577-022-00763-8.

Chatterjee, S., R. Kordbacheh, and J. et Sin. 2024. "Extracellular Vesicles: A Novel Mode of Viral Propagation Exploited by Enveloped and Non-Enveloped Viruses." *Microorganisms* 12, no. 2: 274. https://doi.org/10.3390/microorganisms12020274.

Chen, R., Z. Kang, W. Li, et al. 2024. "Extracellular Vesicle Surface Display of αPD-L1 and αCD3 Antibodies via Engineered Late Domain-Based Scaffold to Activate T-Cell Anti-Tumor Immunity." *Journal of Extracellular Vesicles* 13, no. 7: e12490. https://doi.org/10.1002/jev2.12490.

Chen, S., S. Bonifati, Z. Qin, C. St Gelais, and L. Wu. 2019. "SAMHD1 Suppression of Antiviral Immune Responses." *Trends in Microbiology* 27, no. 3: 254–267. https://doi.org/10.1016/j.tim.2018.09.009.

Cortes-Galvez, D., J. A. Dangerfield, and C. Metzner. 2023. "Extracellular Vesicles, and Their Membranes: Exosomes vs. Virus-Related Particles." *Membranes* 13, no. 4: 397. https://doi.org/10.3390/membranes13040397.

Cottingham, M. G., and M. W. Carroll. 2013. "Recombinant MVA Vaccines: Dispelling the Myths." *Vaccine* 31, no. 39: 4247–4251. https://doi.org/10.1016/j.vaccine.2013.03.021.

Couté, Y., C. Bruley, and T. Burger. 2020. "Beyond Target–Decoy Competition: Stable Validation of Peptide and Protein Identifications in Mass Spectrometry-Based Discovery Proteomics." *Analytical Chemistry* 92, no. 22: 14898–14906. https://doi.org/10.1021/acs.analchem.0c00328.

Defourny, K. A. Y. et al. 2024. "Picornavirus Security Proteins Promote the Release of Extracellular Vesicle Enclosed Viruses via the Modulation of Host Kinases." *PLOS Pathogens* 20, no. 4: e1012133. https://doi.org/10.1371/journal.ppat.1012133.

Doceul, V., M. Hollinshead, L. van der Linden, and G. L Smith. 2010. "Repulsion of Superinfecting Virions: A Mechanism for Rapid Virus Spread." *Science* 327, no. 5967: 873–876. https://doi.org/10.1126/science.1183173.

Dodding, M. P., and M. Way. 2009. "Nck- and N-WASP-Dependent Actin-Based Motility Is Conserved in Divergent Vertebrate Poxviruses." *Cell Host & Microbe* 6, no. 6: 536–550. https://doi.org/10.1016/j.chom.2009.10.011.

Elgueta, R., M. J Benson, V. C de Vries, A. Wasiuk, Y. Guo, and R. J Noelle. 2009. "Molecular Mechanism and Function of CD40/CD40L Engagement in the Immune System." *Immunological Reviews* 229, no. 1: 152–172. https://doi.org/10.1111/j.1600-065X.2009.00782.x.

Erbs, P., A. Findeli, J. Kintz, et al. 2008. "Modified Vaccinia Virus Ankara as a Vector for Suicide Gene Therapy." *Cancer Gene Therapy* 15, no. 1: 18–28. https://doi.org/10.1038/sj.cgt.7701098.

Foloppe, J., J. Kempf, N. Futin, et al. 2019. "The Enhanced Tumor Specificity of TG6002, an Armed Oncolytic Vaccinia Virus Deleted in Two Genes Involved in Nucleotide Metabolism." *Molecular Therapy—Oncolytics* 14: 1–14. https://doi.org/10.1016/j.omto.2019.03.005.

Fournillier, A., E. Gerossier, A. Evlashev, et al. 2007. "An Accelerated Vaccine Schedule with a Poly-Antigenic hepatitis C Virus MVA-Based Candidate Vaccine Induces Potent, Long Lasting and in Vivo Cross-Reactive T Cell Responses." *Vaccine* 25, no. 42: 7339–7353. https://doi.org/10.1016/j.vaccine.2007.08.020.

Frischknecht, F., V. Moreau, S. Röttger, et al. 1999. "Actin-Based Motility of Vaccinia Virus Mimics Receptor Tyrosine Kinase Signalling." *Nature* 401, no. 6756: 926–929. https://doi.org/10.1038/44860.

Fu, Y., L. Zhang, F. Zhang, et al. 2017. "Exosome-Mediated miR-146a Transfer Suppresses Type I Interferon Response and Facilitates EV71 Infection." *PLOS Pathogens* 13, no. 9: e1006611. https://doi.org/10.1371/journal.ppat.1006611.

Fujita, S., A. Eguchi, J. Okabe, et al. 2006. "Sendai Virus-Mediated Gene Delivery Into Hepatocytes via Isolated Hepatic Perfusion." *Biological and Pharmaceutical Bulletin* 29, no. 8: 1728–1734. https://doi.org/10.1248/bpb.29.1728.

Gelderblom, H., and D. Madeley. 2018. "Rapid Viral Diagnosis of Orthopoxviruses by Electron Microscopy: Optional or a Must?" *Viruses* 10, no. 4: 142. https://doi.org/10.3390/v10040142.

Gomes, F. G., A. C Andrade, M. Wolf, et al. 2022. "Synergy of Human Platelet-Derived Extracellular Vesicles With Secretome Proteins Promotes Regenerative Functions." *Biomedicines* 10, no. 2: 238. https://doi.org/10.3390/biomedicines10020238.

Greening, D. W., R. Xu, A. Ale, C. E Hagemeyer, and W. Chen. 2023. "Extracellular Vesicles as Next Generation Immunotherapeutics." *Seminars in Cancer Biology* 90: 73–100. https://doi.org/10.1016/j.semcancer.2023.02.002.

Grosenbach, D. W., D. O. Ulaeto, and D. E. Hruby. 1997. "Palmitylation of the Vaccinia Virus 37-kDa Major Envelope Antigen." *Journal of Biological Chemistry* 272, no. 3: 1956–1964. https://doi.org/10.1074/jbc.272.3.1956.

Hassan, Z., N. D Kumar, F. Reggiori, and G. Khan. 2021. "How Viruses Hijack and Modify the Secretory Transport Pathway." *Cells* 10, no. 10: 2535. https://doi.org/10.3390/cells10102535.

Henson, B. W., E. M Perkins, J. E Cothran, and P. Desai. 2009. "Self-Assembly of Epstein-Barr Virus Capsids." *Journal of Virology* 83, no. 8: 3877–3890. https://doi.org/10.1128/JVI.01733-08.

Hirigoyen, U., C. Guilbaud, M. Krejbich, et al. 2024. "Oncolytic Viruses Alter the Biogenesis of Tumor Extracellular Vesicles and Influence Their Immunogenicity." *Molecular Therapy: Oncology* 32, no. 4: 200887. https://doi.org/10.1016/j.omton.2024.200887.

Honeychurch, K. M., Yang, G., R. Jordan, and D. E Hruby. 2007. "The Vaccinia Virus F13L YPPL Motif Is Required for Efficient Release of Extracellular Enveloped Virus." *Journal of Virology* 81, no. 13: 7310–7315. https://doi.org/10.1128/jvi.00034-07.

Huttunen, M., J. Samolej, R. J Evans, et al. 2021. "Vaccinia Virus Hijacks ESCRT-Mediated Multivesicular Body Formation for Virus Egress." *Life Science Alliance* 4, no. 8: e202000910. https://doi.org/10.26508/lsa.202000910.

Iša, P., A. Pérez-Delgado, I. R Quevedo, S. López, and C. F Arias. 2020. "Rotaviruses Associate With Distinct Types of Extracellular Vesicles." *Viruses* 12, no. 7: 763. https://doi.org/10.3390/v12070763.

Jiang, W., P. Ma, L. Deng, et al. 2020. "Hepatitis A Virus Structural Protein pX Interacts With ALIX and Promotes the Secretion of Virions and Foreign Proteins Through Exosome-Like Vesicles." *Journal of Extracellular Vesicles* 9, no. 1: 1716513. https://doi.org/10.1080/20013078.2020.1716513.

Kalluri, R., and V. S. LeBleu. 2020. "The Biology, Function, and Biomedical Applications of Exosomes." *Science* 367, no. 6478: eaau6977. https://doi.org/10.1126/science.aau6977.

Kumar, M. A., S. K Baba, H. Q Sadida, et al. 2024. "Extracellular Vesicles as Tools and Targets in Therapy for Diseases." *Signal Transduction and Targeted Therapy* 9, no. 1: 27. https://doi.org/10.1038/s41392-024-01735-1.

Lin, C.-L., C. S Chung, H. G Heine, and W. Chang. 2000. "Vaccinia Virus Envelope H3L Protein Binds to Cell Surface Heparan Sulfate and Is Important for Intracellular Mature Virion Morphogenesis and Virus Infection in Vitro and in Vivo." *Journal of Virology* 74, no. 7: 3353–3365. https://doi.org/10.1128/JVI.74.7.3353-3365.2000.

20013078, 2026, 6, Downloaded from https://isevjournals.onlinelibrary.wiley.com/doi/10.1002/jev2.70307 by Cochrane France, Wiley Online Library on [19/06/2026]. See the Terms and Conditions (https://onlinelibrary.wiley.com/terms-and-conditions) on Wiley Online Library for rules of use; OA articles are governed by the applicable Creative Commons License

Liu, C., X. Liu, X. Xiang, et al. 2022. "A Nanovaccine for Antigen Self-Presentation and Immunosuppression Reversal as a Personalized Cancer Immunotherapy Strategy." *Nature Nanotechnology* 17, no. 5: 531–540. https://doi.org/10.1038/s41565-022-01098-0.

Liu, L., R. Chavan, and M. B. Feinberg. 2008. "Dendritic Cells are Preferentially Targeted Among Hematolymphocytes by Modified Vaccinia Virus Ankara and Play a key Role in the Induction of Virus-Specific T Cell Responses in Vivo." *BMC Immunology* 9, no. 1: 15. https://doi.org/10.1186/1471-2172-9-15.

Lyu, X., T. Yamano, K. Nagamori, et al. 2025. "Direct Delivery of Immune Modulators to Tumour-Infiltrating Lymphocytes Using Engineered Extracellular Vesicles." *Journal of Extracellular Vesicles* 14, no. 4: e70035. https://doi.org/10.1002/jev2.70035.

Martin, C., G. Ligat, and C. E. Malnou. 2024. "The Yin and the Yang of Extracellular Vesicles During Viral Infections." *Biomedical Journal* 47, no. 5: 100659. https://doi.org/10.1016/j.bj.2023.100659.

Martin-Jaular, L., N. Nevo, J. P Schessner, et al. 2021. "Unbiased Proteomic Profiling of Host Cell Extracellular Vesicle Composition and Dynamics Upon HIV-1 Infection." *The EMBO Journal* 40, no. 8: e105492. https://doi.org/10.15252/embj.2020105492.

Matsumoto, A., M. Asuka, Y. Takahashi, and Y. Takakura. 2020. "Antitumor Immunity by Small Extracellular Vesicles Collected From Activated Dendritic Cells Through Effective Induction of Cellular and Humoral Immune Responses." *Biomaterials* 252: 120112. https://doi.org/10.1016/j.biomaterials.2020.120112.

McConnell, R. E., and M. J. Tyska. 2007. "Myosin-1a Powers the Sliding of Apical Membrane Along Microvillar Actin Bundles." *The Journal of Cell Biology* 177, no. 4: 671–681. https://doi.org/10.1083/jcb.200701144.

McInnes, C. J., I. K Damon, G. L Smith, et al. 2023. "ICTV Virus Taxonomy Profile: Poxviridae 2023: This Article Is Part of the ICTV Virus Taxonomy Profiles Collection." *Journal of General Virology* 104, no. 5: 1–2. https://doi.org/10.1099/jgv.0.001849.

Medina-Echeverz, J., M. Hinterberger, M. Testori, et al. 2019. "Synergistic Cancer Immunotherapy Combines MVA-CD40L Induced Innate and Adaptive Immunity With Tumor Targeting Antibodies." *Nature Communications* 10, no. 1: 5041. https://doi.org/10.1038/s41467-019-12998-6.

Minh, A., and A. A. Kamen. 2021. "Critical Assessment of Purification and Analytical Technologies for Enveloped Viral Vector and Vaccine Processing and Their Current Limitations in Resolving Co-Expressed Extracellular Vesicles." *Vaccines* 9, no. 8: 823. https://doi.org/10.3390/vaccines9080823.

Mirlekar, B., and Y. Pylayeva-Gupta. 2021. "IL-12 Family Cytokines in Cancer and Immunotherapy." *Cancers* 13, no. 2: 167. https://doi.org/10.3390/cancers13020167.

Mohamed, A. H., T. Abaza, Y. A Youssef, et al. 2025. "Extracellular Vesicles: From Intracellular Trafficking Molecules to Fully Fortified Delivery Vehicles for Cancer Therapeutics." *Nanoscale Advances* 7, no. 4: 934–962. https://doi.org/10.1039/d4na00393d.

Moulin, C., M. J F. Crupi, C. S Ilkow, J. C Bell, and S. Boulton. 2023. "Extracellular Vesicles and Viruses: Two Intertwined Entities." *International Journal of Molecular Sciences* 24, no. 2: 1036. https://doi.org/10.3390/ijms24021036.

Muralidharan-Chari, V., J. Clancy, C. Plou, et al. 2009. "ARF6-Regulated Shedding of Tumor Cell-Derived Plasma Membrane Microvesicles." *Current Biology* 19, no. 22: 1875–1885. https://doi.org/10.1016/j.cub.2009.09.059.

Ng, C. Y., L. T Kee, M. E Al-Masawa, et al. 2022. "Scalable Production of Extracellular Vesicles and Its Therapeutic Values: A Review." *International Journal of Molecular Sciences* 23, no. 14: 7986. https://doi.org/10.3390/ijms23147986.

Nolte-'t Hoen, E., T. Cremer, R. C Gallo, and L. B Margolis. 2016. "Extracellular Vesicles and Viruses: Are They Close Relatives?" *Proceedings of the National Academy of Sciences* 113, no. 33: 9155–9161. https://doi.org/10.1073/pnas.1605146113.

Nolte-'t Hoen, E. N. M., S. I Buschow, S. M Anderton, W. Stoorvogel, and M. H Wauben. 2009. "Activated T Cells Recruit Exosomes Secreted by Dendritic Cells via LFA-1." *Blood* 113, no. 9: 1977–1981. https://doi.org/10.1182/blood-2008-08-174094.

Ohs, I., M. van den Broek, K. Nussbaum, et al. 2016. "Interleukin-12 Bypasses Common Gamma-Chain Signalling in Emergency Natural Killer Cell Lymphopoiesis." *Nature Communications* 7, no. 1: 13708. https://doi.org/10.1038/ncomms13708.

Pail, O., M. J Lin, T. Anagnostou, B. D Brown, and J. D Brody. 2025. "Cancer Vaccines and the Future of Immunotherapy." *The Lancet* 406, no. 10499: 189–202. https://doi.org/10.1016/S0140-6736(25)00553-7.

Palmulli, R., M. Couty, M. C Piontek, et al. 2024. "CD63 Sorts Cholesterol Into Endosomes for Storage and Distribution via Exosomes." *Nature Cell Biology* 26, no. 7: 1093–1109. https://doi.org/10.1038/s41556-024-01432-9.

Perez-Riverol, Y., J. Bai, C. Bandla, et al. 2022. "The PRIDE Database Resources in 2022: A Hub for Mass Spectrometry-Based Proteomics Evidences." *Nucleic Acids Research* 50, no. D1: D543–D552. https://doi.org/10.1093/nar/gkab1038.

Pokorny, L., J. J Burden, D. Albrecht, et al. 2024. "The Vaccinia Chondroitin Sulfate Binding Protein Drives Host Membrane Curvature to Facilitate Fusion." *EMBO Reports* 25, no. 3: 1310–1325. https://doi.org/10.1038/s44319-023-00040-2.

Pols, M. S., and J. Klumperman. 2009. "Trafficking and Function of the Tetraspanin CD63." *Experimental Cell Research* 315, no. 9: 1584–1592. https://doi.org/10.1016/j.yexcr.2008.09.020.

Rademacher, M. J., A. Cruz, M. Faber, et al. 2021. "Sarcoma IL-12 Overexpression Facilitates NK Cell Immunomodulation." *Scientific Reports* 11, no. 1: 8321. https://doi.org/10.1038/s41598-021-87700-2.

Rajan, S., D. S. Kudryashov, and E. Reisler. 2023. "Actin Bundles Dynamics and Architecture." *Biomolecules* 13, no. 3: 450. https://doi.org/10.3390/biom13030450.

Ramos, R. N., C. Tosch, F. Kotsias, et al. 2022. "Pseudocowpox Virus, a Novel Vector to Enhance the Therapeutic Efficacy of Antitumor Vaccination." *Clinical & Translational Immunology* 11, no. 5: e1392. https://doi.org/10.1002/cti2.1392.

Roberts, K. L., A. Breiman, G. C Carter, et al. 2009. "Acidic Residues in the Membrane-Proximal Stalk Region of Vaccinia Virus Protein B5 are Required for Glycosaminoglycan-Mediated Disruption of the Extracellular Enveloped Virus Outer Membrane." *Journal of General Virology* 90, no. 7: 1582–1591. https://doi.org/10.1099/vir.0.009092-0.

Sapoznikov, A., S. Kozlovski, N. Levi, et al. 2023. "Dendritic Cell ICAM-1 Strengthens Synapses With CD8 T Cells but Is Not Required for Their Early Differentiation." *Cell Reports* 42, no. 8: 112864. https://doi.org/10.1016/j.celrep.2023.112864.

Schioppa, T., C. Gaudenzi, G. Zucchi, et al. 2024. "Extracellular Vesicles at the Crossroad Between Cancer Progression and Immunotherapy: Focus on Dendritic Cells." *Journal of Translational Medicine* 22, no. 1: 691. https://doi.org/10.1186/s12967-024-05457-4.

Seclì, L., G. Leoni, V. Ruzza, et al. 2023. "Personalized Cancer Vaccines Go Viral: Viral Vectors in the Era of Personalized Immunotherapy of Cancer." *International Journal of Molecular Sciences* 24, no. 23: 16591. https://doi.org/10.3390/ijms242316591.

Segura, E., C. Nicco, B. Lombard, et al. 2005. "ICAM-1 on Exosomes From Mature Dendritic Cells Is Critical for Efficient Naive T-Cell Priming." *Blood* 106, no. 1: 216–223. https://doi.org/10.1182/blood-2005-01-0220.

Shen, Z., G. Reznikoff, G. Dranoff, and K. L Rock. 1997. "Cloned Dendritic Cells can Present Exogenous Antigens on Both MHC Class I and Class II Molecules." *Journal of Immunology* 158, no. 6: 2723–2730.

Sidhom, K., P. O. Obi, and A. Saleem. 2020. "A Review of Exosomal Isolation Methods: Is Size Exclusion Chromatography the Best Option?."

20013078, 2026, 6, Downloaded from https://isevjournals.onlinelibrary.wiley.com/doi/10.1002/jev2.70307 by Cochrane France, Wiley Online Library on [19/06/2026]. See the Terms and Conditions (https://onlinelibrary.wiley.com/terms-and-conditions) on Wiley Online Library for rules of use; OA articles are governed by the applicable Creative Commons License

International Journal of Molecular Sciences 21, no. 18: 6466. https://doi.org/10.3390/ijms21186466.

Singh, B., M. Fredriksson Sundbom, U. Muthukrishnan, et al. 2025. "Extracellular Histones as Exosome Membrane Proteins Regulated by Cell Stress." *Journal of Extracellular Vesicles* 14, no. 2: e70042. https://doi.org/10.1002/jev2.70042.

Sinha, S., D. Hoshino, N. H Hong, et al. 2016. "Cortactin Promotes Exosome Secretion by Controlling Branched Actin Dynamics." *Journal of Cell Biology* 214, no. 2: 197–213. https://doi.org/10.1083/jcb.201601025.

Soares, M., M. M Pinto, R. J Nobre, et al. 2023. "Isolation of Extracellular Vesicles From Human Follicular Fluid: Size-Exclusion Chromatography versus Ultracentrifugation." *Biomolecules* 13, no. 2: 278. https://doi.org/10.3390/biom13020278.

Spehner, D., and R. Drillien. 2008. "Extracellular Vesicles Containing Virus-Encoded Membrane Proteins are a Byproduct of Infection With Modified Vaccinia Virus Ankara." *Virus Research* 137, no. 1: 129–136. https://doi.org/10.1016/j.virusres.2008.07.003.

Stack, J., and A. G. Bowie. 2012. "Poxviral Protein A46 Antagonizes Toll-Like Receptor 4 Signaling by Targeting BB Loop Motifs in Toll-IL-1 Receptor Adaptor Proteins to Disrupt Receptor:Adaptor Interactions." *Journal of Biological Chemistry* 287, no. 27: 22672–22682. https://doi.org/10.1074/jbc.M112.349225.

Sun, J., C. Liu, R. Peng, et al. 2020. "Cryo-EM Structure of the Varicella-Zoster Virus A-Capsid." *Nature Communications* 11, no. 1: 4795. https://doi.org/10.1038/s41467-020-18537-y.

Symons, A., and L. Smith. 1995. "Vaccinia Virus Encodes a Soluble Type I Interferon Receptor of Novel Structure and Broad Species Specificity." *Cell* 81, no. 4: 551–560.

Thomas, I. J., L. G Petrich de Marquesini, R. Ravanan, et al. 2007. "CD86 has Sustained Costimulatory Effects on CD8 T Cells." *The Journal of Immunology* 179, no. 9: 5936–5946. https://doi.org/10.4049/jimmunol.179.9.5936.

Travieso, T., J. Li, S. Mahesh, J. Mello, and M. Blasi. 2022. "The use of Viral Vectors in Vaccine Development." *npj Vaccines* 7, no. 1: 75. https://doi.org/10.1038/s41541-022-00503-y.

Usacheva, A., R. Smith, R. Minshall, et al. 2001. "The WD Motif-Containing Protein Receptor for Activated Protein Kinase C (RACK1) Is Required for Recruitment and Activation of Signal Transducer and Activator of Transcription 1 Through the Type I Interferon Receptor." *Journal of Biological Chemistry* 276, no. 25: 22948–22953. https://doi.org/10.1074/jbc.M100087200.

Vanderplasschen, A., E. Mathew, M. Hollinshead, R. B Sim, and G. L Smith. 1998. "Extracellular Enveloped Vaccinia Virus Is Resistant to Complement Because of Incorporation of Host Complement Control Proteins into Its Envelope." *Proceedings of the National Academy of Sciences* 95, no. 13: 7544–7549. https://doi.org/10.1073/pnas.95.13.7544.

Van Deun, J., P. Mestdagh, R. Sormunen, et al. 2014. "The Impact of Disparate Isolation Methods for Extracellular Vesicles on Downstream RNA Profiling." *Journal of Extracellular Vesicles* 3, no. 1: 24858. https://doi.org/10.3402/jev.v3.24858.

Van Niel, G., G. D'Angelo, and G. Raposo. 2018. "Shedding Light on the Cell Biology of Extracellular Vesicles." *Nature Reviews Molecular Cell Biology* 19, no. 4: 213–228. https://doi.org/10.1038/nrm.2017.125.

Welsh, J. A., D. C I. Goberdhan, L. O'Driscoll, et al. 2024. "Minimal Information for Studies of Extracellular Vesicles (MISEV2023): From Basic to Advanced Approaches." *Journal of Extracellular Vesicles* 13, no. 2: e12404. https://doi.org/10.1002/jev2.12404.

Wieczorek, S., F. Combes, C. Lazar, et al. 2017. "DAPAR & ProStaR: Software to Perform Statistical Analyses in Quantitative Discovery Proteomics." *Bioinformatics* 33, no. 1: 135–136. https://doi.org/10.1093/bioinformatics/btw580.

Wolffe, E. J., E. Katz, A. Weisberg, and B. Moss. 1997. "The A34R Glycoprotein Gene is Required for Induction of Specialized Actin-Containing Microvilli and Efficient Cell-to-Cell Transmission of Vaccinia Virus." *Journal of Virology* 71, no. 5: 3904–3915. https://doi.org/10.1128/jvi.71.5.3904-3915.1997.

Xu, M., J. Ji, D. Jin, et al. 2023. "The Biogenesis and Secretion of Exosomes and Multivesicular Bodies (MVBs): Intercellular Shuttles and Implications in Human Diseases." *Genes & Diseases* 10, no. 5: 1894–1907. https://doi.org/10.1016/j.gendis.2022.03.021.

Yang, C., Y. Xue, Y. Duan, C. Mao, and M. Wan. 2024. "Extracellular Vesicles and Their Engineering Strategies, Delivery Systems, and Biomedical Applications." *Journal of Controlled Release* 365: 1089–1123. https://doi.org/10.1016/j.jconrel.2023.11.057.

Yao, F., L. Y Long, Y. Z Deng, et al. 2014. "RACK1 Modulates NF-κB Activation by Interfering With the Interaction Between TRAF2 and the IKK Complex." *Cell Research* 24, no. 3: 359–371. https://doi.org/10.1038/cr.2013.162.

Yin, W., D. Duluc, H. Joo, et al. 2016. "Therapeutic HPV Cancer Vaccine Targeted to CD40 Elicits Effective $CD8^+$ T-Cell Immunity." *Cancer Immunology Research* 4, no. 10: 823–834. https://doi.org/10.1158/2326-6066.CIR-16-0128.

Zheng, W., J. Rädler, H. Sork, et al. 2023. "Identification of Scaffold Proteins for Improved Endogenous Engineering of Extracellular Vesicles." *Nature Communications* 14, no. 1: 4734. https://doi.org/10.1038/s41467-023-40453-0.

Zhou, X., T. Xu, C. Li, et al. 2025. "Potentiating Anti-Tumor Immunity by Re-Engaging Immune Synapse Molecules." *Cell Reports Medicine* 6, no. 3: 101975. https://doi.org/10.1016/j.xcrm.2025.101975.

Supporting Information

Additional supporting information can be found online in the Supporting Information section.

Supplementary Figure 1: UC, velocity gradient and SEC do not separate EVs from infectious poxvirus particles. (A) Cryo-EM images of particles retrieved in 100k g pellet after UC of culture medium from non-infected (left) or VV_{COP}-infected human peripheral blood mononuclear cells (PBMC), showing the presence of EVs (black stars) and electron dense viral particles (black arrows). Scale bar: 100 nm. B–C) EVs were isolated either by velocity gradient (B) or by SEC (C) from the supernatant of non-infected PBMCs (mock) or infected by VV_{COP} at a multiplicity of infection of 1 (MOI = 1). In each fraction, particles were quantified by NTA (top graphs) and virus infectivity was assessed by titration of PFU (bottom graphs). $N = 1$ experiment each. (D) 100 nm filtration coupled to UC is not able to fully remove PCPV infectious particles. (E) Cryo-EM images of stocks from VV_{COP}, MVA and PCPV viruses showing the shape of viral particles (black arrows). Scale bar: 100 nm. **Supplementary Figure 2: Poxvirus infection increases sEVs secretion. (A–E)** NTA quantification of EVs and particles isolated by UC (**A**), immunocapture (**B**), density gradient (**C**), velocity gradient (**D**) or SEC (**E**) from non-infected PBMCs (mock, blue) or infected with VV_{COP} virus (yellow). (**F**) NTA quantification of EVs isolated by UC and filtered at 200 nm or 100 nm from PBMCs infected with either VV_{COP} (yellow), MVA (orange) or PCPV (light blue) virus. **Supplementary Figure 3: Poxvirus infection alters the content of secreted EVs**. Mass spectrometry analysis of the protein content of EVs secreted by PBMCs infected by MVA poxvirus and isolated by UC preceded or not by 100 nm or 200 nm filtration. Mass spectrometry was performed in quadruplicate. (**A)** Gene ontology analysis of the EVs proteins differentially expressed upon poxvirus infection. (**B)** Heat maps showing differentially expressed viral proteins identified in UC pellet with or without filtration (100 nm or 200 nm). label corresponds to MVA Uniprot ID (VVcop ortholog). The heat map of viral proteins complements the heat map in Figure 2F and applies the same color code, log10 transformation, and normalization of abundance

20013078, 2026, 6, Downloaded from https://isevjournals.onlinelibrary.wiley.com/doi/10.1002/jev2.70307 by Cochrane France, Wiley Online Library on [19/06/2026]. See the Terms and Conditions (https://onlinelibrary.wiley.com/terms-and-conditions) on Wiley Online Library for rules of use; OA articles are governed by the applicable Creative Commons License

values. **Supplementary Figure 4: Multi-armed therapeutic poxvirus impairs tumor growth. (A)** Protocol used to determine the anti-tumoral potential of MVA virus encoding different therapeutic payloads. Viruses were injected intravenously 5-, 12- and 19-days post E.G7-OVA tumor cell injection and tumor growth was monitored for 42 days. (**B)** tumor growth curves of individual mice treated with PBS, with empty virus or with virus encoding the OVA antigens alone or in combination with IL-12, CD40L or both. Arrows indicate the injection days. One curve represents one mouse, $n = 5$ to 10 mice per group, in $N = 1$ experiment. The PBS and empty MVA groups present a significantly higher tumor growth rate than all the other groups from Day 11 to 28 (after this point, there were not enough mice alive in the empty MVA group). The virus encoding the three payloads (OVA, CD40L and IL12, pink) had a significant lower tumor growth rate than the virus encoding only OVA or than the virus encoding both OVA and CD40L (respective adjusted *P*-Values = 0.046 to 0.048 Day 21 to 25; 0.017 to 0.041 - from day 25 to 30). Supplementary Figure 5: EVs isolated from therapeutic virus-infected DC activate and stimulate anti-tumoral cytotoxic T cells *in vitro*. (A) Quantification of the number of $CD8^+$ T cells per generation (from G0 to G6) following stimulation with positive control (anti-CD3/CD28 antibodies) or with EVs. One curve represents one experiment. (B) $CD8^+$ OVA-specific T cells proliferation by EVs relies on SIINFEKL presentation by MHC-I. T cells were incubated with EVs isolated by UC from DC2.4 cells infected with a triple armed MVA (^{armed}iDC-EVs) and with increasing concentrations of anti-SIINFEKL/MHCI blocking antibody. Mean of $n = 2$ values per condition. (C) Tumor growth curves of individual mice bearing E.G7-OVA tumors and treated with PBS (black, left), or with EVs isolated by UC from cells infected with empty MVA virus (blue, right) as in Figure 5. Arrows indicate the injection days. One curve represents one mouse, $n = 8$ mice per group. Data shown for the PBS group (left graph) are also shown in Figure 5B. D) Cytometry quantification of the proportion of OVA-specific $CD8^+$ T cells isolated from the circulating blood of tumor-bearing mice treated with a triple armed MVA virus or with EVs isolated from non-infected DC2.4 cells (DC-EVs UC) by UC, or from DC2.4 cells infected with a triple armed MVA by UC (^{armed}iDC-EVs) or by SEC (^{armed}iDC-EVs SEC for EVs and ^{armed}iDC-Prots SEC for the soluble fraction). Blood was collected at day 21 from mice described in Figure 5. $n = 1$ to 6 mice per group, in $N = 1$ experiment.

20013078, 2026, 6, Downloaded from https://isevjournals.onlinelibrary.wiley.com/doi/10.1002/jev2.70307 by Cochrane France, Wiley Online Library on [19/06/2026]. See the Terms and Conditions (https://onlinelibrary.wiley.com/terms-and-conditions) on Wiley Online Library for rules of use; OA articles are governed by the applicable Creative Commons License